Excitations and Bose-Einstein condensation in liquid ^{4}He

A. R. Sakhel and H. R. Glyde
Department of Physics and Astronomy, University of Delaware, Newark, Delaware 19716, USA
(Received 31 January 2004; published 21 October 2004)

We present a model of the dynamic structure factor $S(\mathbf{Q},\omega)$ of ^{4}He that reproduces the basic features of the temperature dependence of $S(\mathbf{Q},\omega)$ as observed in inelastic-neutron scattering measurements. Wave vectors Q beyond the roton ($Q>2.0$ Å^{-1}) are considered. The model is able to reproduce the decrease in the intensity of the single excitation (phonon-roton) peak in $S(\mathbf{Q},\omega)$ with an increase of temperature (T) in the range $0.6 \leqslant T \leqslant 2.1$ K. All vertices and interactions are assumed temperature independent, and only the condensate fraction $n_0(T)$ changes with T. Also, it reproduces a second peak observed at higher energy (ω) which represents the single excitation intensity lying in the two excitation band. The model is based on the formulation of $S(\mathbf{Q},\omega)$ of Gavoret and Nozières. In this formulation, the dynamic susceptibility, χ, is separated into a singular part involving the condensate and a regular part involving states above the condensate $\chi=\chi_S+\chi'_R$. The weight of the phonon-roton peak in χ_S is proportional to $n_0(T)$ and the phonon-roton peak disappears completely from χ in the normal phase where $n_0(T)=0$. Using sum rule arguments, the condensate fraction can be estimated from the data giving values in good agreement with accurate measurements at SVP and with Monte Carlo calculations.

DOI: 10.1103/PhysRevB.70.144511 PACS number(s): 67.40.Db, 67.40.Bz

I. INTRODUCTION

We explore the temperature dependence of the dynamic structure factor $S(\mathbf{Q},\omega)$ of liquid ^{4}He at wave vectors beyond the roton. The purpose is to see whether the weight of the phonon-roton (p-r) mode in $S(\mathbf{Q},\omega)$ scales with the condensate fraction, $n_0(T)$, or not. Equivalently, the aim is to show that the existence of an observable phonon-roton (p-r) mode at higher wave vectors in superfluid ^{4}He follows from the existence of a condensate. This is done by using a rigorous expression for $S(\mathbf{Q},\omega)$ in which the condensate $n_0(T)$ appears explicitly. All parameters in the expression are held independent of T except $n_0(T)$ and the Bose function $n_B(\omega)=(e^{\beta\hbar\omega}-1)^{-1}$, where $\beta=(kT)^{-1}$ and k is Boltzmann's constant.

To set the stage, we show the observed energy dispersion curve, ω_Q, of the single p-r excitation in superfluid ^{4}He at low temperature in Fig. 1. This shows the "phonon," "maxon," "roton" and "beyond the roton" regions of the dispersion curve. The energy at the "roton" wave vector, Q_R, is $\omega_Q=\Delta$ and a well defined single p-r mode exists out to wave vectors $Q=3.6$ Å^{-1}. As Q increases beyond Q_R, the weight, z_Q, of the p-r mode in $S(\mathbf{Q},\omega)$ decreases until z_Q vanishes at $Q=3.6$ Å^{-1}. The two p-r band starts at energy 2Δ and continues up to twice the maxon energy. There is a repulsion between the single and pair p-r components[1] which prevents the single p-r energy from exceeding 2Δ. We will focus on the single p-r self energy Σ^{12} arising from this interaction.

At wave vectors "beyond the roton" ($2.5 \leqslant Q \leqslant 3.6$ Å^{-1}; see Fig. 1), the momentum ($\hbar Q$) and energy transfer ($\hbar\omega$) in $S(\mathbf{Q},\omega)$ are at their highest value relative to the interactions in the fluid and yet there is still a p-r mode at low temperature. In this case, we anticipate the best separation between the single p-r and the multiexcitation components of $S(\mathbf{Q},\omega)$. In this region, we anticipate that an expression for $S(\mathbf{Q},\omega)$ separated into a part that contains $n_0(T)$ and the single p-r mode plus a part that describes the multi-excitation component will be most clearly identifiable. At low ω in the "phonon" and "roton" regions (see Fig. 1), the single p-r mode and the "total" density components are largely combined into a single peak. Thus at lower energy it is more difficult to identify the temperature dependence arising from $n_0(T)$ and separate it from the remaining components of $S(\mathbf{Q},\omega)$.

At wave vectors "beyond the roton," $S(\mathbf{Q},\omega)$ has three components at low temperature (see Fig. 2). There is a sharp peak (at $\omega \approx 1.5$ meV in Fig. 2) which is identified as the

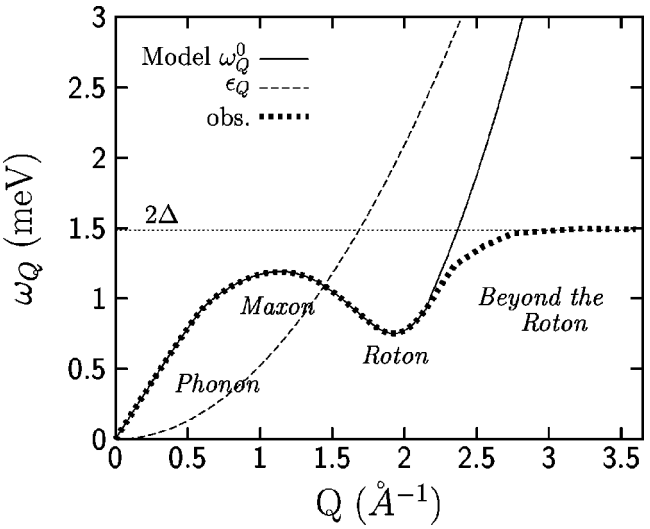

FIG. 1. The observed p-r energy dispersion curve (solid squares), a model p-r dispersion curve, ω_Q^0, used in our calculations (solid line), and the free particle energy $\epsilon_Q=\hbar Q^2/2m$ (dotted lines). 2Δ is twice the roton energy. Four regions of the p-r spectrum are identified: the phonon ($Q<0.7$ Å^{-1}), the maxon, ($Q\sim 1.1$ Å^{-1}), the roton ($Q\sim 1.9$ Å^{-1}) and beyond the roton ($Q\geqslant 2.4$ Å^{-1}) regions.

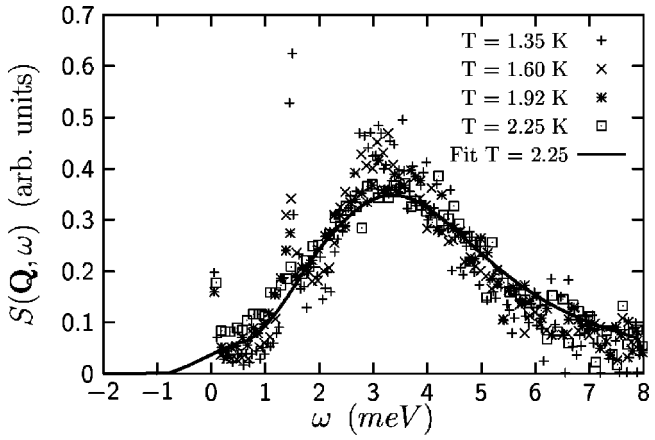

FIG. 2. Observed dynamic structure factor $S(\mathbf{Q},\omega)$ of liquid ^{4}He at SVP at $Q=2.65$ Å^{-1} vs the energy transfer, ω, and $T=1.35$, 1.60, 1.92, and 2.25 K (from Ref. 10). The solid line is a fit of our model to the data at the highest temperature $T=2.25$ K.

single p-r mode shown in Fig. 1. There is a broader peak centered at $\omega\approx 3$ meV in Fig. 2. This is interpreted[2,3] as the single p-r response that lies in the two p-r band ($\omega>2\Delta$). Third, $S(\mathbf{Q},\omega)$ has a very broad component that extends up to energies of 7–8 meV. The weight of the first two components of $S(\mathbf{Q},\omega)$ decreases strongly with increasing temperature and these components are not observable as separate components at $T>T_\lambda$ in the normal phase where $n_0(T)=0$. The third component, especially at higher ω, is largely independent of temperature and the same in superfluid and normal ^{4}He.

To describe $S(\mathbf{Q},\omega)$ we employ an expression derived by Gavoret and Nozières.[4] In this expression, the dynamic susceptibility $\chi(Q)$ of a Bose fluid containing a condensate is formally separated into two parts,

$$\chi(Q)=\chi_S(Q)+\chi_R'(Q), \tag{1}$$

where $Q=\mathbf{Q},\omega$. $\chi_S(Q)$, the "singular part," includes all terms which involve the condensate ($p=0$ state) and $\chi_S\propto n_0(T)$. $\chi_R'(Q)$, the "regular part," involves the fluid above the condensate only (states $p\neq 0$). The $\chi_S(Q)$ at $Q>Q_R$ has a structure which reproduces the sharp and broad peaks in $S(\mathbf{Q},\omega)$ (as shown in Fig. 2) well while $\chi_R'(\mathbf{Q},\omega)$ is a broad function of ω. The goal is to explore how well the temperature dependence of $S(\mathbf{Q},\omega)$ at several Q values can be reproduced by this expression allowing only $n_0(T)$ and the Bose function $n_B(\omega)$ to depend on T. For $n_0(T)$ we use the result observed[5] at SVP,

$$n_0(T)=n_0(0)\left[1-\left(\frac{T}{T_\lambda}\right)^\gamma\right], \tag{2}$$

with $n_0(0)=7.25\%$ and $\gamma=5.50$ with a scale adjustment at $P=20$ bars. In this way the aim is to reveal how the existence of the p-r mode depends on the existence of a condensate — at least at higher wave vectors. Anticipating the results, we find that the T dependence of $S(\mathbf{Q},\omega)$ can be very well reproduced allowing only $n_0(T)$ to vary with T. To reproduce, in addition, the temperature dependence of $S(\mathbf{Q},\omega)$ at low ω ($\omega\leqslant 1$ meV) (below the p-r peaks considered here), we found it was necessary to include a temperature dependent half width Γ_Q to the p-r energies. We used the observed $\Gamma_Q(T)$.

Early measurements of $S(\mathbf{Q},\omega)$ at wave vectors beyond the roton ($Q\geqslant 2.5$ Å^{-1}) are summarized by Cowley and Woods.[6,7] Their data among other properties gives values of the weights, z_Q, in the sharp peak of $S(\mathbf{Q},\omega)$ at wave vectors "beyond the roton." They showed that this weight decreases with increasing Q beyond the roton until $z_Q\rightarrow 0$ at $Q=3.6$ Å^{-1}, the end point of the p-r excitations. Above $Q=3.6$ Å^{-1}, $S(\mathbf{Q},\omega)$ is a broad function of ω centered just below the free atom recoil frequency $\omega_R=\hbar Q^2/2m$. Smith *et al.*[8] reported similar measurements on ^{4}He under pressure.

Fåk and Andersen,[9] Fåk *et al.*[2] and Fåk and Bossy[3] have presented a systematic series of measurements of the temperature dependence of $S(\mathbf{Q},\omega)$ for $2.3\leqslant Q\leqslant 4.0$ Å^{-1}. Their data shows clearly that as Q increases beyond $Q\geqslant 2.3$ Å^{-1} the weight, z_Q, in the sharp p-r peak decreases with increasing Q. They showed that this weight is transferred to the broad peak lying at energies in the two excitation band ($\omega>2\Delta$) as Q increases. Again at $Q\geqslant 3.6$ Å^{-1}, $z_Q=0$. Their data also showed that the weight in both the sharp and broad peak decreases with increasing temperature and that both peaks disappear at $T\geqslant T_\lambda$. They fitted models to their data which suggest that the weight in these two peaks is proportional to the condensate fraction, $n_0(T)$, as noted below. Glyde *et al.*[10] and Pearce *et al.*[11] made high energy resolution measurements of $S(\mathbf{Q},\omega)$ beyond the roton. For $Q\gtrsim 2.8$ Å^{-1}, these provide accurate and precise values of the "p-r" energies, ω_Q, the position of the sharp peak. They show specifically that the single p-r energy, ω_Q, never exceeds 2Δ, twice the roton energy. For $Q\geqslant 2.8$ Å^{-1}, $\omega_Q\simeq 2\Delta=1.48$ meV at SVP, for example. The data also shows that the weights in the sharp and broad peaks have the general Q and temperature dependence noted above by Fåk *et al.*[2] and Fåk and Bossy[3] (see Fig. 2).

There have been many theories and models[1,12–20] of $S(\mathbf{Q},\omega)$ at wavevectors beyond the roton. At low wavevectors, up to the roton region, the p-r mode at low T can be interpreted as a single density excitation.[12] With modern refinements accurate values of ω_Q can be obtained within this interpretation.[21] Historically, Pitaevskii[1] first focused on Q values beyond the roton. He showed that the p-r energy ω_Q could not exceed 2Δ. As a result, he noted that the p-r dispersion curve would bend over at $Q\approx 2.5$ Å^{-1} and become flat at higher Q as shown in Fig. 1. He described the p-r response by a single particle Green's function,

$$G(\mathbf{Q},\omega)=\frac{1}{\omega^2-(\omega_Q^0)^2-2\omega_Q^0\Sigma^{12}(\mathbf{Q},\omega)}, \tag{3}$$

as we use here in Eq. (26) below. In Eq. (3), ω_Q^0 is a model initial single p-r energy of the type calculated by Feynman and Cohen which does not explicitly include the interaction between the single p-r and pairs of p-r excitations (see Fig. 1). The self energy $\Sigma_{12}=n_0J\chi J$ in this $G(\mathbf{Q},\omega)$ leads to a repulsion between the single mode and the pair p-r response

(χ) which begins at energy 2Δ. As a result of the repulsion, the p-r energy ω_Q "bends over" beyond the roton and $\omega_Q \leqslant 2\Delta$ out to the end point. He noted that since the $\Im m(\chi^0(\mathbf{Q},\omega))$ goes abruptly from zero to a finite value at $\omega=2\Delta$, $\Re e(\chi^0(\mathbf{Q},\omega))$ will have a logarithmic singularity at $\omega=2\Delta$, as shown later in Fig. 17(a).

All subsequent formulations of response at wave vectors "beyond the roton" have, as here, used this expression for $G(\mathbf{Q},\omega)$—with different variations of the model single p-r energy ω_Q^0 and the pair dynamic susceptibility χ. In these formulations, the three-point interaction J is often written as $g_3(\mathbf{Q})=\sqrt{n_0}nJ(\mathbf{Q})$ where $n_0=N_0/N$ and $n=N/V$ is the number density. Equation (3) has the same form as G for single phonons in solids including the coupling to pairs of phonons ($\chi=G_2$) via the cubic anharmonic term ($J=V_3$). Equation (1) was also used by Jackson[15] at lower Q values to obtain the single p-r energy, the sharp peak in $G(\mathbf{Q},\omega)$ at $\omega<2\Delta$ where $\Im m(\Sigma^{12}(\mathbf{Q},\omega))=0$, and the second resonance at higher ω ($\omega\approx 4\Delta$) where $\Im m(\Sigma^{12}(\mathbf{Q},\omega))\neq 0$.

Ruvalds and Zawadowski[13] and Zawadowski *et al.*[14] examined the pair p-r response (χ) which is observed in light scattering from liquid ^{4}He. $\chi(\mathbf{Q},\omega)$ was expressed in terms of independent pair propagation, χ'^0, within a random phase approximation (RPA), an equation of the form (A27). χ'^0 is represented by various independent pair models, usually the first term of Eq. (28) with $n_1=n_2=0$ and $A=1$ or analytic models. The interaction between the G and pair p-r response via Σ^{12} was investigated in detail. They showed that singularities in the pair χ^0 could be removed by adding a very small imaginary part to ω_Q which we follow here. Zawadowski *et al.* presented an explicit formulation of both $\chi(\mathbf{Q},\omega)$ and $G(\mathbf{Q},\omega)$ emphasizing the interaction between them via Σ^{12}. They emphasized that the hybridization of the single p-r mode with a two-roton "mode" via Σ^{12} would lead to the observed bending over of the single p-r mode beginning at $Q=2.2$ Å^{-1} and a mixed character of the mode for $Q\geqslant 2.5$ Å^{-1}. They also noted that $I(\mathbf{Q})$ $(g_4(\mathbf{Q}))$ could be negative. An attractive interaction arising from a negative g_4 leads to two-roton bound states when the two interacting excitations are rotons.

Bedell *et al.*[16] evaluated g_4 extensively and found that g_4 was chiefly negative at Q values of interest. They reformulated many properties using their improved values of g_4. Explicitly, calculations of $I(\mathbf{Q})=g_4(\mathbf{Q})$ using a T-matrix and beginning from a pair potential in liquid ^{4}He find that $I(\mathbf{Q})$ oscillates in sign with Q at higher Q ($Q\geqslant 2$ Å^{-1}). These oscillations in $I(\mathbf{Q})$ at even higher Q values ($5-10$ Å^{-1}) are observed in neutron scattering data.[22]

Glyde[23] evaluated the total χ in Eq. (1) as a function of temperature using a model based on the dielectric formulation.[22,24] This included both G and the regular density, χ_R'. At $T>T_\lambda$, the total χ reduces to χ_R' and χ_R' can be determined from data in the normal phase, concepts we use here. As here, the sharp p-r peak in G has a weight proportional to $n_0(T)$ and Pearce *et al.*[11] show that this model reproduces the observed temperature dependence well.

Juge and Griffin[18] explored the temperature dependence of the single p-r $G(\mathbf{Q},\omega)$ and pair p-r χ_2 interacting via Σ^{12} without evaluating $S(\mathbf{Q},\omega)$ explicitly. Fåk and Bossy[3] considered a simplified version of the Gavoret-Nozières expression Eq. (1) to model the temperature dependence of $S(\mathbf{Q},\omega)$. They particularly used a χ_R' that was determined by fitting to data in the normal phase. Juge and Griffin[18] and Fåk and Bossy[3] began with a model p-r dispersion curve of the Feynman-Cohen (FC) form to describe ω_Q^0 before Σ^{12} is introduced which we adopt here (see Fig. 1). Szwabinski and Weyrauch[20] have derived and evaluated the Gavoret and Nozières expression consistently at $T=0$ K. Recent work is discussed more fully in Sec. V.

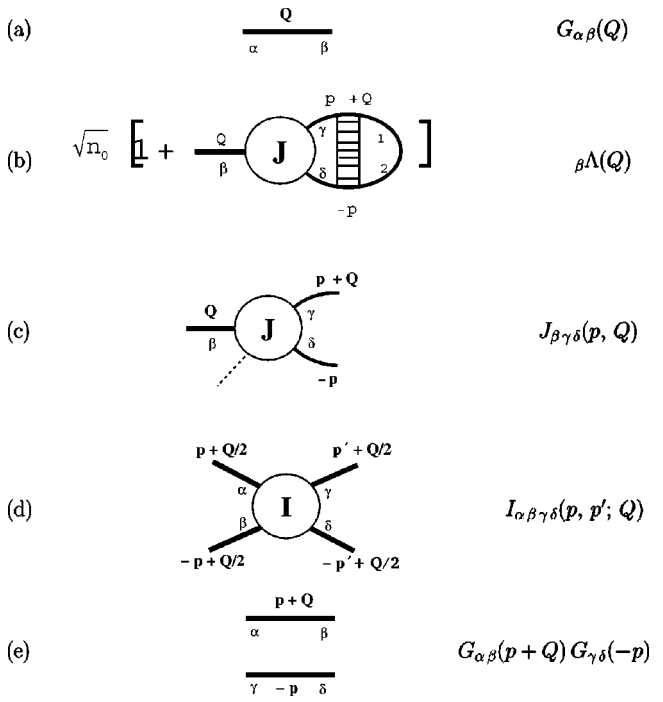

FIG. 3. Basic components of the model of $S(\mathbf{Q},\omega)$: (a) single particle Boson Green's function; (b) vertex appearing in Eq. (6); (c) three-point interaction; (d) four-point interaction; and (e) pair propagation (particle-hole) function.

In Sec. II we introduce the model and derive the basic expressions used in our analysis. In Sec. III we present our results and compare our model with experiment. In Sec. IV we analyze some of the important expressions in our model. In Sec. V we discuss the model, connect to previous work and list our conclusions.

II. THE MODEL

We consider a fluid of N Bosons in a volume V that has a condensate fraction $n_0=N_0/N$ in the zero momentum ($p=0$) state. We begin with the exact expression for the dynamic susceptibility, $\chi(Q)$, of this Bose fluid in the form, $\chi(Q)=\chi_S(Q)+\chi_R'(Q)$, or

$$\chi(Q)=\Lambda_\alpha(Q)G_{\alpha\beta}(Q)_\beta\Lambda(Q)+\chi_R'(Q), \tag{4}$$

where $Q=\mathbf{Q},\omega$. In Eqs. (1) and (4), $\chi(Q)$ has been separated into a singular part $\chi_S(Q)$ which involves the condensate and a regular part $\chi_R'(\mathbf{Q},\omega)$ which involves states ($p\neq 0$) above the condensate only. This separation was made originally by

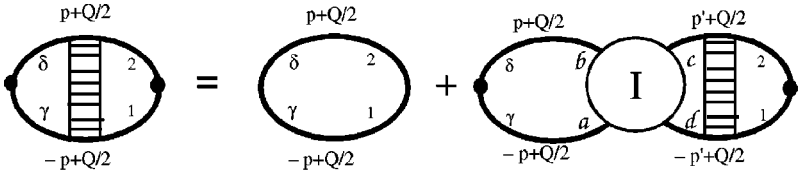

FIG. 4. Diagrammatic representation of Eq. (7).

$$\chi'_{\gamma 1\delta 2}(p,Q) = \chi'^{0}_{\gamma 1\delta 2}(p,Q) + \int d\bar{p}'\chi'^{0}_{\gamma a\delta b}(p,Q)\, I_{abcd}(p,p',Q)\,\chi'_{c1d2}(p',Q)$$

Gavoret and Nozières[4] at $T=0$ K and is reproduced here for finite T in the Appendix. In normal ^{4}He, where there is no condensate, $\chi_S(Q)=0$. In Eq. (4), $G_{\alpha\beta}(Q)$ is the single Boson Green's function [see Fig. 3(a)] defined by

$$G_{\alpha\beta}(\mathbf{p},\tau) = -\langle T_\tau a_p^\alpha(\tau) a_p^{\dagger\beta}(0)\rangle, \tag{5}$$

which has four components ($\alpha=1,2$; $\beta=1,2$) with $a_p^\alpha = a_p(\alpha=1)$ and $a_p^\alpha = a_{-p}^\dagger(\alpha=2)$. In Eq. (5), τ is an imaginary time and T_τ is the time ordering operator. The vertex [see Fig. 3(b)] is

$$_\beta\Lambda(Q) = \sqrt{n_0}\left[1 + \int d\bar{p} J_{\beta\gamma\delta}(p,Q)\chi'_{\gamma 1\delta 2}(p,Q)\right], \tag{6}$$

where $J_{\beta\gamma\delta}(p,Q)$ is the three-point interaction, defined in Fig. 3(c) [$J_{\beta\gamma\delta}(p,Q)=I_{\beta\beta\gamma\delta}(0,p;Q)$], $p=\mathbf{p},\omega_p$. $\chi'_{\gamma 1\delta 2}(p,Q)$ is the dynamic susceptibility (DS) for a specific momentum p ($p\neq 0$) and indices $\gamma 1\delta 2$ given by

$$\chi'_{\gamma 1\delta 2}(p,Q) = \chi'^{0}_{\gamma 1\delta 2}(p,Q) + \int d\bar{p}'\chi'^{0}_{\gamma a\delta b}(p,Q) I_{abcd}(p,p',Q)\chi'_{c1d2}(p',Q). \tag{7}$$

In Eq. (7), I_{abcd} is the usual four-point Boson-Boson interaction [Fig. 3(d)] and χ'^0 is the zeroth-order, independent boson DS,

$$\chi'^{0}_{abcd}(p,Q) = G_{ab}(-p)G_{cd}(p+Q), \tag{8}$$

[see Fig. 3(e)] where again $G_{\alpha\beta}(\mathbf{p},\omega)$ is the full four component Green's function. Equation (7) is depicted in Fig. 4 and

$$\int d\bar{p} \equiv \frac{1}{V}\Sigma_p\left(-\frac{1}{\beta\hbar}\right)\Sigma_n \tag{9}$$

is a sum over momentum p and frequencies $i\omega_n$. The four terms in $\chi_S(Q)$ are represented diagrammatically in Fig. 5.

The $\chi'_R(Q)$ is given by the usual expression for the DS for a normal Bose fluid,

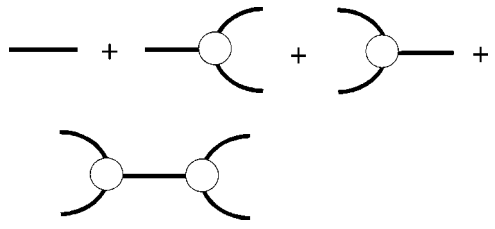

FIG. 5. Diagrammatic representation of $\Lambda G\Lambda$.

$$\chi'_R(Q) = \frac{V}{N}\left[\chi'^{0}_R(Q) + \int d\bar{p}\int d\bar{p}'\chi'^{0}_{2a1b}(p,Q)I_{abcd}(p,p',Q)\chi'_{c1d2}(p',Q)\right], \tag{10}$$

where

$$\chi'^{0}_R(Q) = \int d\bar{p}[\chi'^{0}_{2112}(p,Q) + \chi'^{0}_{2211}(p,Q)] \tag{11}$$

is the zeroth order (independent Boson) DS.

The equations (1) to (11) define the full $\chi(Q)$ (see the Appendix). Our goal is to test how well the temperature dependence of the dynamic structure factor,

$$S(\mathbf{Q},\omega) = -\frac{[n_B(\omega)+1]}{\pi}\Im m(\chi(\mathbf{Q},\omega)), \tag{12}$$

can be reproduced by allowing only the Bose functions $n_B(\omega)$ and the condensate fraction $n_0(T)$ to depend on temperature. In a second model, we will allow the p-r energies $\omega^0_{\mathbf{Q}}+i\Gamma_{\mathbf{Q}}$ to have a temperature dependent half width $\Gamma_{\mathbf{Q}}(T)$.

A. Approximations

To reduce $\chi(Q)$ in Eq. (4) to a computationally tractable form, we make the following approximations. We assume that the four-point and three-point interactions are independent of the indices, of $\mathbf{p}$ and of energy ω,

$$I_{\alpha\beta\gamma\delta}(p,p',Q) \to I(\mathbf{Q}),$$

$$J_{\alpha\beta\gamma}(p,Q) \to J(\mathbf{Q}). \tag{13}$$

The $I(\mathbf{Q})$ and $J(\mathbf{Q})$ will be taken as temperature independent constants at each $\mathbf{Q}$. Given approximation (13),

$$\chi(Q) = \Lambda(Q)G(Q)\Lambda(Q) + \chi'_R(Q), \tag{14}$$

where

$$G(Q) \equiv \sum_{\alpha\beta} G_{\alpha\beta}(Q), \tag{15}$$

$$\Lambda(Q) = \sqrt{n_0}[1 + J(\mathbf{Q})\chi'_\Lambda(Q)], \tag{16}$$

$$\chi'_\Lambda(Q) = \chi'^{0}_\Lambda(Q) + \chi'^{0}_\Lambda(Q)I(\mathbf{Q})\chi'_\Lambda(Q), \tag{17}$$

and

$$\chi'^{0}_{\Lambda}(Q) = \int d\bar{p} \sum_{\alpha\beta} \chi'^{0}_{\alpha 1 \beta 2}(p,Q). \tag{18}$$

Equation (17) for $\chi'_{\Lambda}(Q)$ is not quite an exact reduction of Eq. (7) given approximation (13). Some truncation of indices in the interaction term is also required to arrive at Eq. (17).

In most previous work, the interactions $g_3(\mathbf{Q}) = \sqrt{n_0} n J(\mathbf{Q})$ and $g_4(\mathbf{Q}) = I(\mathbf{Q})$ have been used. We prefer to use $J(\mathbf{Q})$ since $n_0(T)$ then appears explicitly in the expressions and $J(\mathbf{Q})$ can be held independent of temperature in models.

B. Green's function, $G_{\alpha\beta}(Q)$

To evaluate $G_{\alpha\beta}$, we write the self energy Σ as a sum of two parts, $\Sigma = \Sigma^{FC} + \Sigma^{12}$. The Σ^{FC} includes all of the interactions of the single quasiparticle (single p-r) with the fluid except the interaction of the single p-r mode with pairs of p-r excitations, described by Σ^{12}. We are using the fact that $G_{\alpha\beta}(Q)$ and $\chi(Q)$ share common poles[22,24] to identify the mode described by G with the p-r mode. The first part of Σ is denoted Σ^{FC} since Feynman and Cohen (FC)[12] in their original calculation included all processes (in principle) except Σ^{12}. The FC energy, ω^0_Q, is phonon like at low Q, has a minimum at wave vectors in the roton region, Q_R, and goes to a free particle energy $\omega^0_Q \to \epsilon_Q = \hbar Q^2/2m$ at high Q. Explicitly, we write

$$G^{-1}_{\alpha\beta} = (g^0_{\alpha\beta})^{-1} - \Sigma^{FC}_{\alpha\beta} - \Sigma^{12}_{\alpha\beta} \equiv g^{-1}_{\alpha\beta} - \Sigma^{12}_{\alpha\beta}, \tag{19}$$

where $g^0_{\alpha\beta}$ is the free Bose Green's function and $g^{-1}_{\alpha\beta} = (g^0_{\alpha\beta})^{-1} - \Sigma^{FC}_{\alpha\beta}$ is the FC Green's function, which has the FC energy noted above.

As the FC energy, ω^0_Q, we use the observed energy for Q values up to the roton wave vector, Q_R following Juge and Griffin[18] and Fåk and Bossy.[3] For $Q > Q_R$, we allow ω^0_Q to go smoothly to $\hbar Q^2/2m$ at high Q. We require ω^0_Q at $Q = Q_R$ to be the observed ω_Q so that the roton energy, Δ, is "correct" and the two p-r excitation band which starts at twice the roton energy, 2Δ will begin at the "correct" energy.

The Σ^{12} is most important at Q values where ω^0_Q is close to 2Δ (i.e., at the maxon and $Q > Q_R$). Σ^{12} provides a repulsion between the sharp part of the single p-r response (the single p-r peak at $Q > Q_R$) and the two p-r response. This repulsion leads to the flattening of the observed single p-r energy at $Q \geqslant 2.5$ Å^{-1} and keeps this energy below 2Δ. The model FC energy we use, the observed p-r energy and 2Δ are depicted in Fig. 1.

We assume that the FC Green's functions $g_{\alpha\beta}(\mathbf{Q}, i\omega_n)$ take the Bogoliubov form

$$g_{11}(\mathbf{Q}, i\omega_n) = \left(\frac{u_Q^2}{i\omega_n - \omega^0_Q} - \frac{v_Q^2}{i\omega_n + \omega^0_Q} \right),$$

$$g_{12}(\mathbf{Q}, i\omega_n) = -u_Q v_Q \left(\frac{1}{i\omega_n - \omega^0_Q} - \frac{1}{i\omega_n + \omega^0_Q} \right),$$

$$= g_{21}(\mathbf{Q}, i\omega_n), \tag{20}$$

and $g_{22}(\mathbf{Q}, i\omega_n) = g_{11}(\mathbf{Q}, -i\omega_n)$. With this structure,

$$g(Q) \equiv \sum_{\alpha\beta} g_{\alpha\beta}(Q) = (u_Q - v_Q)^2 \left(\frac{1}{i\omega_n - \omega^0_Q} - \frac{1}{i\omega_n + \omega^0_Q} \right), \tag{21}$$

and for the Bogoliubov u_Q and v_Q, $(u_Q - v_Q)^2 = \epsilon_Q/\omega^0_Q$ where again $\epsilon_Q = \hbar Q^2/2m$.

We take $u_Q^2 = z_Q$, the observed weight of the single p-r peak in $S(\mathbf{Q}, \omega)$. In $g_{11}(\mathbf{Q}, i\omega_n)$, the first term proportional to u_Q^2 describes the creation of a quasiparticle (qp) with wave vector Q above the condensate. [In $S(\mathbf{Q}, \omega)$ this process corresponds to the neutron exciting a qp out of the condensate ($p = 0$) to a state Q above the condensate.] The second term in $g_{11}(\mathbf{Q}, i\omega_n)$, proportional to v_Q^2, corresponds to annihilation of a qp with wave vector Q (above the condensate) with the qp going into the condensate. Since only 7–8% of the fluid is in the condensate,[5] we expect that $u_Q^2 \ll v_Q^2$ ($v_Q^2 \sim 13.7 u_Q^2$). We found $v_Q^2 = 10.6 u_Q^2$ provided a good fit to data at $T = 0$ K. These values of u_Q^2 and v_Q^2 were also consistent with the relation $(u_Q - v_Q)^2 = \epsilon_Q/\omega^0_Q$.

C. Self energy, Σ^{12}

With the "FC" Green's functions $g_{\alpha\beta}$ determined by Eqs. (20) with "FC" energy ω^0_Q and u_Q and v_Q set, we turn to the remaining single p-r self energy, Σ^{12}. This arises from interaction of the single p-r with pairs of p-r's and is[1]

$$\Sigma^{12}_{\alpha\beta}(Q) = n_0 \int d\bar{p} J_{\alpha a b}(p,Q) \chi'^{0}_{abcd}(p,Q) P_{cd\beta}(p,Q), \tag{22}$$

where $P(p,Q)$ is defined in the appendix. We approximate this to

$$\Sigma^{12}_{\alpha\beta}(Q) = n_0 \int d\bar{p} J_{\alpha a b}(p,Q) \chi'^{0}_{abcd} J_{cd\beta}(p,Q). \tag{23}$$

The approximation of (22) to (23) may also be viewed as approximating $\chi'_{abcd}(p,Q)$ by $\chi'^{0}_{abcd}(p,Q)$ in Eq. (23). As in (13), we approximate $J_{\alpha\beta\gamma}(p,Q) \to J(\mathbf{Q})$. Σ^{12} is then independent of indices α and β and we obtain

$$\Sigma^{12}(Q) = n_0 J(\mathbf{Q}) \chi'^{0}_{\Sigma}(Q) J(\mathbf{Q}), \tag{24}$$

where

$$\chi'^{0}_{\Sigma}(Q) = \int d\bar{p} G(-p) G(p+Q) \tag{25}$$

and $G(p) = \Sigma_{\alpha\beta} G_{\alpha\beta}(p)$ as in Eq. (15).

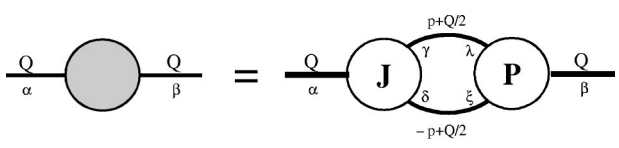

FIG. 6. Diagrammatic representation of Eq. (22) for self energy Σ^{12}.

We use this Σ^{12} to evaluate $G(Q)$ in Eqs. (15) and (19) as $G(Q)^{-1}=g(Q)^{-1}-\Sigma^{12}$ where from Eq. (21) $g(Q)=2\epsilon_Q/[(i\omega_n)^2-(\omega_Q^0)^2]$ giving

$$G(Q)=\frac{2\epsilon_Q}{(i\omega_n)^2-(\omega_Q^0)^2-2\epsilon_Q\Sigma^{12}(\mathbf{Q},i\omega_n)} \tag{26}$$

and $i\omega_n \rightarrow \omega+i\eta$.

D. Zeroth order $\chi'^0(\mathbf{Q},\omega+i\eta)$

In the expressions above, we have three types of zeroth order DS's with different dependences on the indices. In all of these, we approximate the full $G(p)$ by the "FC" $g(p)$. Collecting, the three are

$$\chi'^0_\Lambda(Q)=\int d\overline{p}\sum_\alpha g_{\alpha 1}(-p)\sum_\beta g_{\beta 2}(p+Q) \quad \text{(vertex)},$$

$$\chi'^0_\Sigma(Q)=\int d\overline{p}g(-p)g(p+Q) \quad \text{(self energy)},$$

$$\chi'^0_{abcd}(Q)=\int d\overline{p}g_{ab}(p+Q)g_{cd}(-p) \quad (\chi'_{abcd}). \tag{27}$$

Carrying out the frequency sums indicated in Eq. (9), the χ'^0 all have the same basic structure,

$$\chi'^0(\mathbf{Q},\omega)=\frac{1}{V}\sum_p\left[(n_1+n_2+1)\left(\frac{A}{\omega+i\eta-\omega_1-\omega_2}-\frac{B}{\omega+i\eta+\omega_1+\omega_2}\right)+(n_1-n_2)\times\left(\frac{C}{\omega+i\eta+\omega_1-\omega_2}-\frac{D}{\omega+i\eta-\omega_1+\omega_2}\right)\right], \tag{28}$$

where $\omega_1=\omega_p^0$, $\omega_2=\omega_{p+Q}^0$, $n_1=n_B(\omega_p)$, $n_2=n_B(\omega_{p+Q}^0)$ and A, B, C, D are constants that depend on u_p, u_{p+Q}, v_p, and v_{p+Q}. For example in $\chi'^0_\Sigma(\mathbf{Q},\omega)$, $A=B=C=D=(\epsilon_p/\omega_p^0)(\epsilon_{p+Q}/\omega_{p+Q}^0)$. In $\chi'^0_R(\mathbf{Q},\omega)$, we find

$$A=v_p^2u_{p+Q}^2+H, \quad B=u_p^2v_{p+Q}^2+H,$$

$$C=u_p^2u_{p+Q}^2+H, \quad D=v_p^2v_{p+Q}^2+H, \tag{29}$$

where $H=u_pu_{p+Q}v_pv_{p+Q}$. For $\chi'^0_\Lambda(Q)$ they are

$$A=V_pU_{p+Q}, \quad B=U_pV_{p+Q},$$

$$C=U_pU_{p+Q}, \quad D=V_pV_{p+Q}, \tag{30}$$

where $U_p=u_p^2-u_pv_p$, $V_p=v_p^2-u_pv_p$, $U_{p+Q}=u_{p+Q}^2-u_{p+Q}v_{p+Q}$, and $V_{p+Q}=v_{p+Q}^2-u_{p+Q}v_{p+Q}$. A key point is that to explore the temperature dependence, we have retained all four terms of χ'^0, particularly the second two which include Bose functions and difference processes. In all previous treatments only the first term was retained with Bose functions neglected. Anticipating results, we found that including all four terms made little difference up to temperatures $T=3.0$ K in the ω range of interest here.

The basic procedure is to determine the parameters (ω_Q, u_Q, v_Q, J, I) in $\chi_S=\Lambda G\Lambda$, by fitting to data at low T. These parameters are held constant, independent of T. Specifically, the FC energies ω_Q^0 were selected as shown in Fig. 1. To moderate the singularities in G and χ'^0, we added a small imaginary part to ω_Q^0 ($\omega_Q^0+i\eta$) with $\eta=5$ μeV. This is very approximately 1/10th of the instrumental energy resolution (50 μeV) of the IRIS instrument at the present Q values.

The three-point interaction $J(\mathbf{Q})$ was determined so that the position of the sharp single peak in the single particle $G(\mathbf{Q},\omega)$ given by Eqs. (24) and (26) reproduced the observed p-r energy. That is, $J(\mathbf{Q})$ was determined so that Σ^{12} had the correct magnitude to reproduce the observed p-r energy. The four-point interaction $I(\mathbf{Q})$ was chosen by optimizing the fit of $\chi_S(\mathbf{Q},\omega)$ to $S(\mathbf{Q},\omega)$ observed at low T.

E. Regular response

While the sharp peak at $\omega\approx 1.5$ meV and the broader peak at $\omega\approx 3$ meV in Fig. 2 are attributed to χ_S, the very broad component that extends up to 8 meV in Fig. 2 is interpreted as arising from χ'_R. The regular component, χ'_R, is given by Eqs. (8), (10), and (11). The very broad component is largely independent of temperature and exists in normal liquid ^{4}He. In normal ^{4}He there are no well defined p-r excitations for $Q\geqslant 0.8$ Å^{-1}. The χ'^0_R in χ'_R is therefore not well represented by a two p-r function. It is probably better described by a nearly independent particle-hole response function, with particle energies given approximately by the dashed line in Fig. 1, except at low ω and low T. If χ'_R is to describe the very broad component, χ'^0_R is not the same as the p-r susceptibilities in Eq. (27) that appear in χ_S.

Rather than evaluating $\chi_R(\mathbf{Q},\omega)$ we have determined it by fitting to the data in the normal phase using two models:

MODEL A: DHO function. In this case the whole of $\chi'_R(\mathbf{Q},\omega)$ was represented by a damped harmonic oscillator (DHO) function and the parameters were obtained by fitting to data for normal ^{4}He. The DHO was held independent of T. In this case all T-dependence of $\chi(\mathbf{Q},\omega)$ comes from $\chi_S(\mathbf{Q},\omega)$.

MODEL B: In this model $\chi'_R(\mathbf{Q},\omega)$ in Eq. (10) was written as

$$\chi'_R(\mathbf{Q},\omega)=\Theta(\omega_c-\omega)A(T)\chi'^0_R(\mathbf{Q},\omega)+\Theta(\omega-\omega_c)\times \text{DHO}, \tag{31}$$

where $\Theta(\omega)$ is a step function. For low energies, χ'_R was represented by the zeroth order, two p-r DS, Eq. (11). For energies $\omega>\omega_c$, the interacting part of $\chi'_R(\mathbf{Q},\omega)$ is expected to dominate and was represented by an empirical DHO fitted to the data as in Model A. The energy ω_c and constant $A(T)$ were adjusted to match the absolute value and slope of the two functions at ω_c. ω_c is usually close to the maximum of the imaginary part of $\chi'^0_R(\mathbf{Q},\omega)$. In $\chi'^0_R(\mathbf{Q},\omega)$ and in the other zeroth order susceptibilities, we used energies $\omega_Q^0 \rightarrow \omega_Q^0+i\Gamma_Q(T)$ which had a half width $\Gamma_Q(T)$ given by observed values as a function of temperature. It is the use of

$\chi_R'^0(\mathbf{Q},\omega)$ and incorporating the $\Gamma_Q(T)$ in $\chi_R'^0(\mathbf{Q},\omega)$ that reproduces the observed temperature dependence of $S(\mathbf{Q},\omega)$ at low ω.

III. RESULTS

In this section we compare our model for the DS, $\chi(\mathbf{Q},\omega)$, with data at wave vectors $Q \geq 2.5$ Å^{-1} "beyond the roton." The aim is to identify the role of the condensate in $\chi(\mathbf{Q},\omega)$. $\chi(\mathbf{Q},\omega)$ is separated into a singular part $\chi_S(\mathbf{Q},\omega)$ which is proportional to $n_0(T)$ and a regular part $\chi_R'(\mathbf{Q},\omega)$ as shown in Eq. (4). The $\chi_R'(\mathbf{Q},\omega)$ is determined by a fit to data in the normal phase ($T > T_\lambda$) where $n_0(T)$ and $\chi_S(\mathbf{Q},\omega)$ are zero. The singular component $\Lambda G \Lambda$ which is proportional to $n_0(T)$ is zero for $T > T_\lambda$ where $n_0 = 0$. The parameters in $\chi_S = \Lambda G \Lambda$ are determined by fitting the total χ to data at the lowest temperature available (usually $T = 0.6$ K). All parameters are held independent of T except the condensate fraction $n_0(T)$ and the Bose function $n_B(\omega)$ (model A). In a second model (model B) the p-r energies are assigned a half width $\Gamma_Q(T)$ which has the observed temperature dependence.

The calculated $S(\mathbf{Q},\omega)$ has a "very" sharp single particle peak at low T which can be approximated by a Dirac delta function. However, the observed p-r mode at low temperature measured using the IRIS instrument is "broadened" by the instrumental energy resolution of IRIS which is 50 μeV. In order to incorporate this instrumental energy resolution into our calculations of $S(\mathbf{Q},\omega)$, we convoluted the calculated $S(\mathbf{Q},\omega)$ containing the "sharp" low energy single particle peak with a resolution function that represents the instrumental broadening of IRIS. Following standard procedures, this resolution function was obtained by fitting a suitable function to the observed single particle peak at $T = 0.6$ K.

In Fig. 7, data by Pearce *et al.*[11] at p = 20 bar pressure where $T_\lambda = 1.92$ K are shown as crosses. The model $S(\mathbf{Q},\omega)$ arising from $\chi_R'(\mathbf{Q},\omega)$ alone, which is fitted to the data at $T = 2.1$ K, is shown as the thick solid line. This thick solid line is reproduced in all frames as well as at $T = 2.1$ K to illustrate the difference between $S(\mathbf{Q},\omega)$ above and below T_λ. The thin solid line shows the full model $\chi = \Lambda G \Lambda + \chi_R'$ at three temperatures $T < T_\lambda$. At $T = 0.6$ K, the thin solid line clearly reproduces the sharp, single excitation peak well. It also reproduces the broader peak observed at higher ω ($\omega \approx 3$ meV). The model intensity (thin solid line) in the broader peak is somewhat less than the observed intensity. As T is increased, the intensity in the sharp peak and broad peak decreases. At $T = 2.1$ K there is clearly no intensity in either peak. The temperature dependence in the model follows from the decrease in $n_0(T)$ with increasing T. This clearly reproduces the basic observed T dependence of $S(\mathbf{Q},\omega)$. Figure 8 shows the same comparison with data at $Q = 3.0$ Å^{-1}. Thus the basic structure of Eq. (4) and the simple parametrization of its temperature dependence explains the chief features of the data.

The model given by the thin solid line in Figs. 7 and 8 shows three discrepancies with experiment. First, the intensity in the sharp peak is too low at $T = 1.7$ K. Second, the peak position of the model sharp peak (thin solid line) moves to higher ω as temperature is increased (especially at $T = 1.7$ K) a finding also noted by Fåk and Bossy.[3] In contrast the observed peak position is largely independent of T. Third, at low T, the observed intensity is very small at low $\omega \leq 1.2$ meV. The observed intensity at low ω grows as T increases and is substantial at $T = 2.1$ K. This increase of observed intensity at low ω with increasing T is not reproduced by the model. It is not reproduced essentially because the $\chi_R'(\mathbf{Q},\omega)$ was held independent of T.

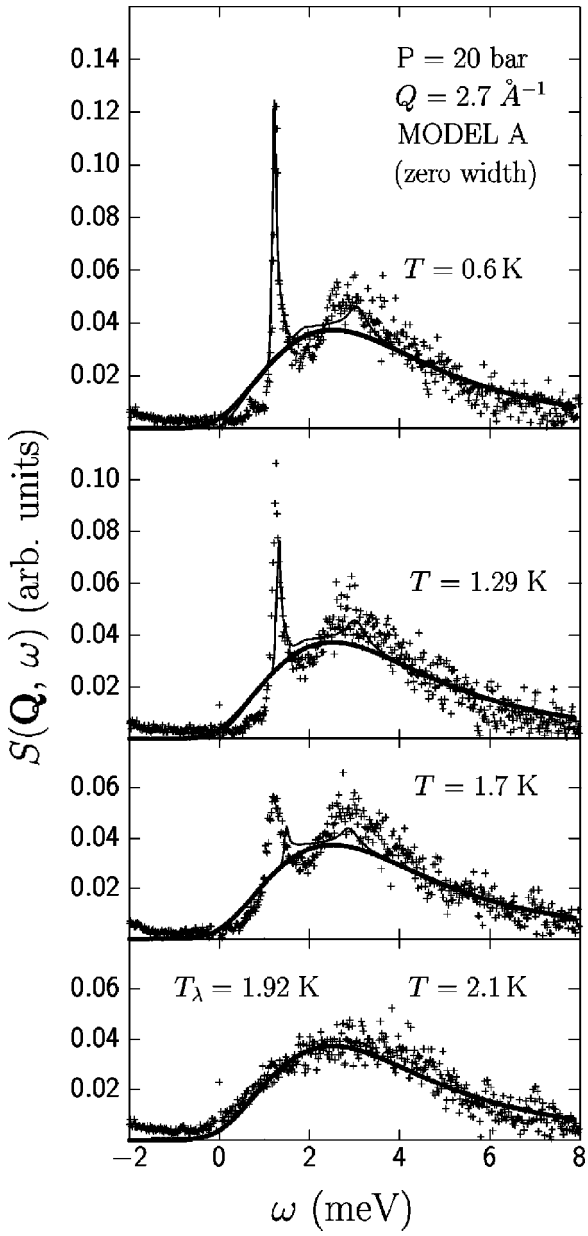

FIG. 7. $S(\mathbf{Q},\omega)$ of liquid ^{4}He at p = 20 bar for $Q = 2.7$ Å^{-1}. The thin solid line is the calculated $S(\mathbf{Q},\omega)$ at temperatures $T = 0.6$, 1.29 and 1.7 K. The thick solid line is a DHO fitted to data at $T = 2.1$ K. The crosses are data from Ref. 11.

To address the issue of the temperature dependence of $S(\mathbf{Q},\omega)$ at low ω, we represented $\chi_R'(\mathbf{Q},\omega)$ by Eq. (31). In Eq. (31), $\chi_R'(\mathbf{Q},\omega)$ at low ω is given by $\chi_R'^0(\mathbf{Q},\omega)$, the inde-

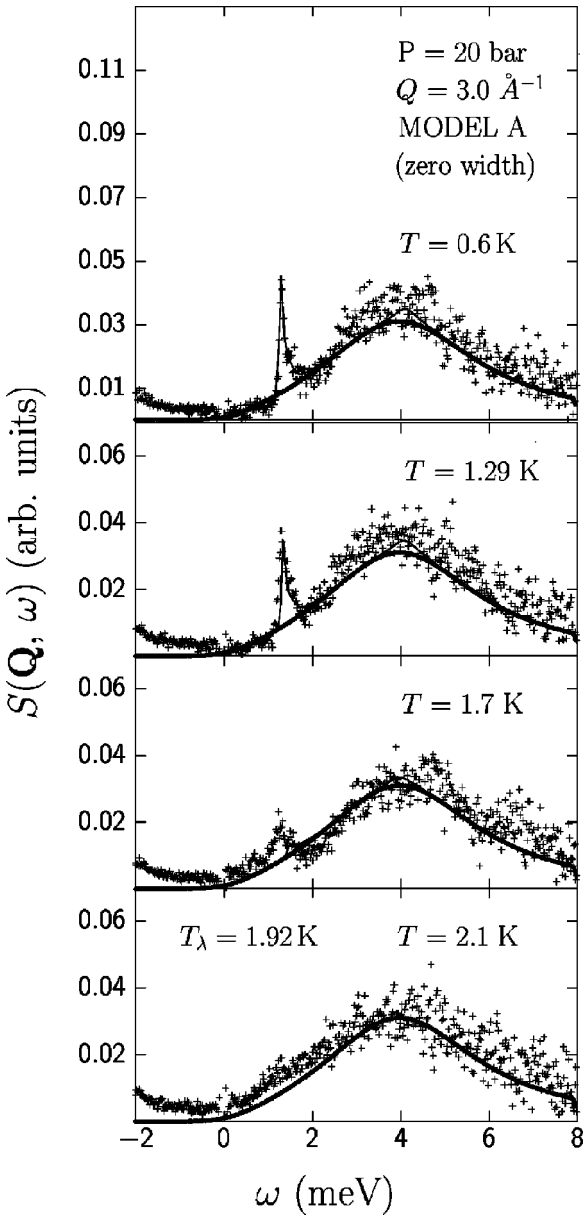

FIG. 8. The same as in Fig. 7 but $Q=3.0$ Å^{-1}.

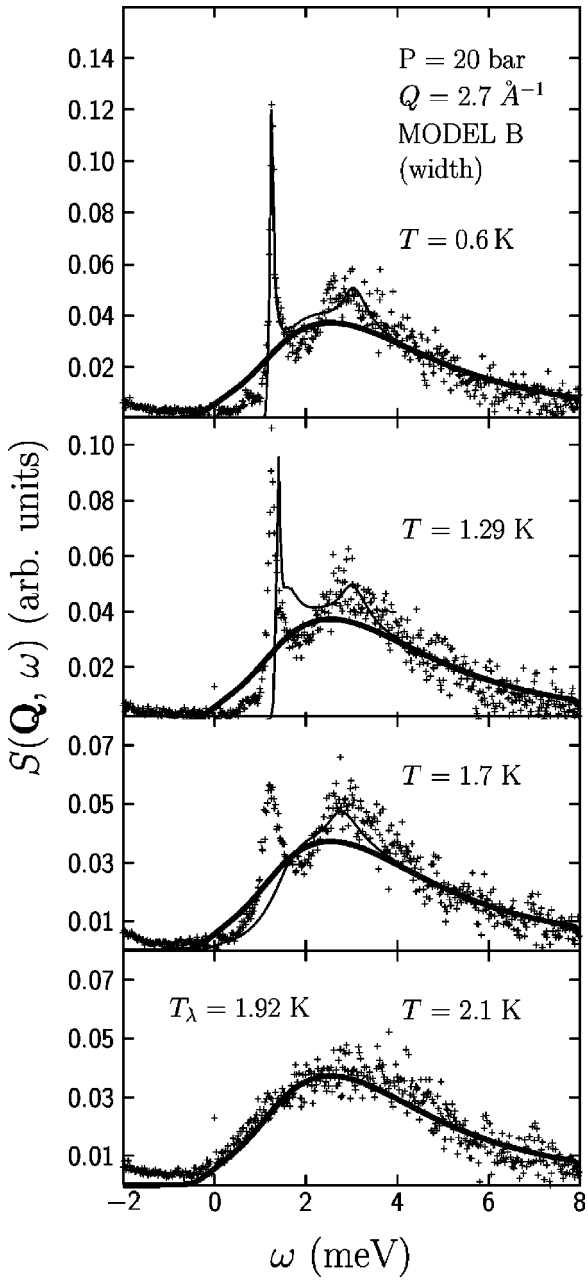

FIG. 9. The same as Fig. 7 except that p-r energies ω_Q^0 having a half width $\Gamma_Q(T)$ fitted to the observed $\Gamma_Q(T)$ are used throughout and $\chi'_R(\mathbf{Q},\omega)$ is given by *MODEL B*.

pendent two p-r part of $\chi'_R(\mathbf{Q},\omega)$ in Eq. (7). To reproduce the observed T dependence of $S(\mathbf{Q},\omega)$ at low ω, we included a half width $\Gamma_Q(T)$ in the p-r energies $\omega_Q^0 \rightarrow \omega_Q^0 + i\Gamma_Q$ at all Q in all the zeroth order DS's given by Eqs. (27) and (28). We used the observed values of $\Gamma_Q(T)$. The higher ω component is ascribed to the interacting term of $\chi'_R(\mathbf{Q},\omega)$ in Eq. (7) and is represented again by a temperature independent DHO which was again determined by a fit to data in the normal phase.

The thin solid line in Fig. 9 shows the temperature dependence of $S(\mathbf{Q},\omega)$ with the observed $\Gamma_Q(T)$ included. Clearly, at $T=0.6$ K there is zero intensity in the model for $\omega \leqslant 1.2$ meV as is observed. As T increases, the intensity in the model increases for $\omega \leqslant 1.2$ meV largely as observed. This T dependence comes from the $\Gamma_Q(T)$ in the p-r's at lower Q values in $\chi'^0_R(\mathbf{Q},\omega)$. The T dependence arising from the Bose functions in the $\chi'^0(\mathbf{Q},\omega)$ was negligible. Including $\Gamma_Q(T)$ also broadens the single p-r peak somewhat, especially at $T=1.7$ K. Figure 10 shows the same model at $Q=3.0$ Å^{-1}. Thus the temperature dependence of $S(\mathbf{Q},\omega)$ at low ω arises from the widths in the p-r excitations. It does not arise from including the "thermal" terms [proportional to $n_B(\omega)$] in $\chi'^0(\mathbf{Q},\omega)$ of Eq. (28) nor from the Bose factor in Eq. (12).

In Fig. 11 we compare the model $S(\mathbf{Q},\omega)$ which uses Eq. (31) for $\chi'_R(\mathbf{Q},\omega)$ and p-r excitations with the observed half widths $\Gamma_Q(T)$ with data at saturated vapor pressure (SVP). The same basic temperature dependence as seen in Figs. 9 and 10 is obtained. The chief discrepancy is that no single p-r peak is obtained in the model at $T=1.92$ K whereas a small peak is observed.

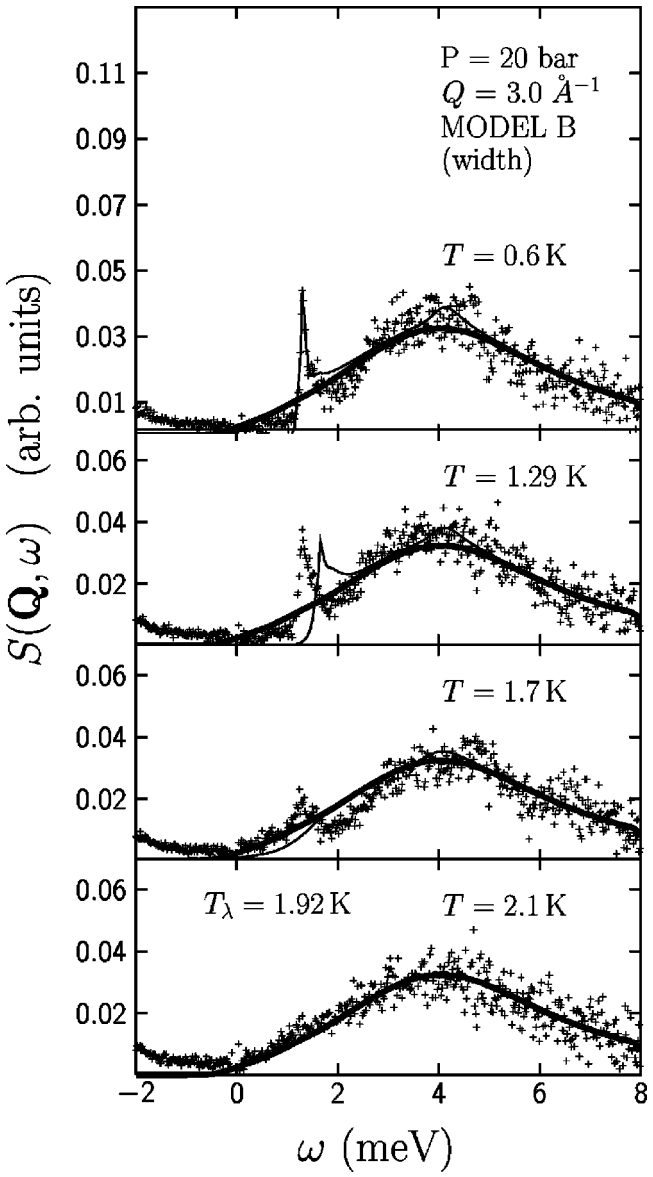

FIG. 10. The same as Fig. 9 but $Q=3.0$ Å^{-1}.

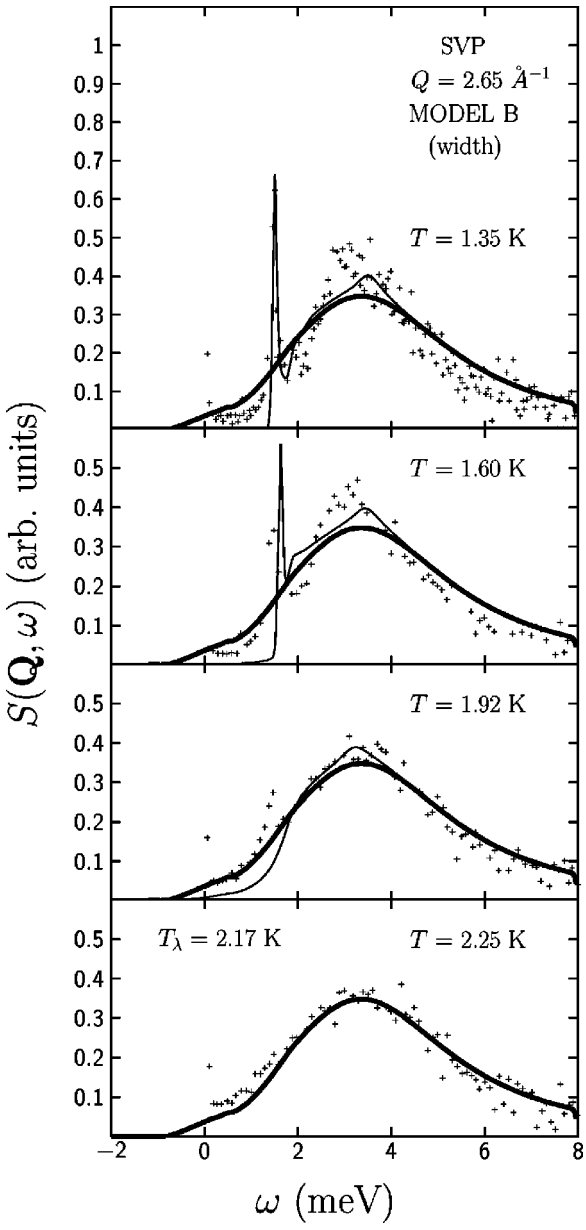

FIG. 11. The same as Fig. 9 for liquid ^{4}He at saturated vapor pressure (SVP) and wave vector $Q=2.65$ Å^{-1}. At SVP, $T_\lambda=2.17$ K. Data from Glyde *et al.* (Ref. 10).

In Fig. 12, the model with $\Gamma_Q(T)=0$ is compared with data taken by Fåk and Bossy[3] for ^{4}He at SVP. In this comparison, the chief discrepancy is that the model p-r peak moves to higher ω as T increases which is not observed.

We now show that the position and magnitude of the p-r peak at higher temperature (e.g., at $T=1.7$ K) can be made to agree with experiment by increasing the magnitude of the three-point interaction $J(\mathbf{Q})$. The upper frame of Fig. 13 reproduces the model results at $T=1.7$ K found in Fig. 9 when $J(\mathbf{Q})$ is held constant independent of T. The middle frame shows the same model when $J(\mathbf{Q})$ is increased by a factor of 1.4 and $\Gamma_Q(T)=0$. In this event, both the p-r peak position and the intensities in the sharp and broad peaks are restored to the observed value. This suggests that either the $J(\mathbf{Q})$ does increase with T or should use a temperature dependent ω_Q^0 as discussed below. The lower frame shows the model with $J(\mathbf{Q})$ increased by a factor of 2 with $\Gamma_Q(T)$ included. In this case the p-r peak position is again approximately correct, but the combined width from $\Gamma_Q(T)$ and the self energy Σ^{12} is too large. We do not believe that $J(\mathbf{Q})$ necessarily depends on temperature. Rather, we illustrate that minor adjustments of the model parameters with temperature can bring the model into agreement with experiment. Particularly, we note below that the roton energy, $\Delta(T)$, does decrease significantly with T. If this decrease were included in the model (i.e., 2Δ decreases with T), we do expect this to prevent the model p-r energies from increasing with T at Q values investigated here. A more detailed analysis of the model appears in the following section.

IV. ANALYSIS

In this section we examine the different components of the singular part of $S(\mathbf{Q},\omega)$, particularly the vertex function

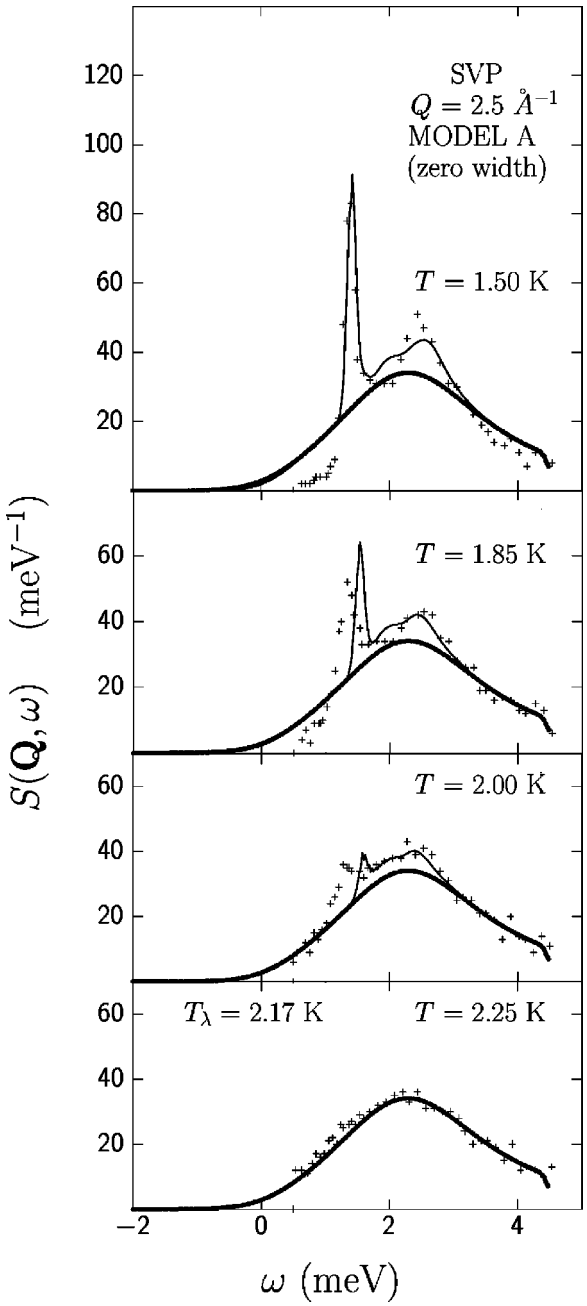

FIG. 12. The same as Fig. 7 compared with data of Fåk and Bossy (Ref. 3).

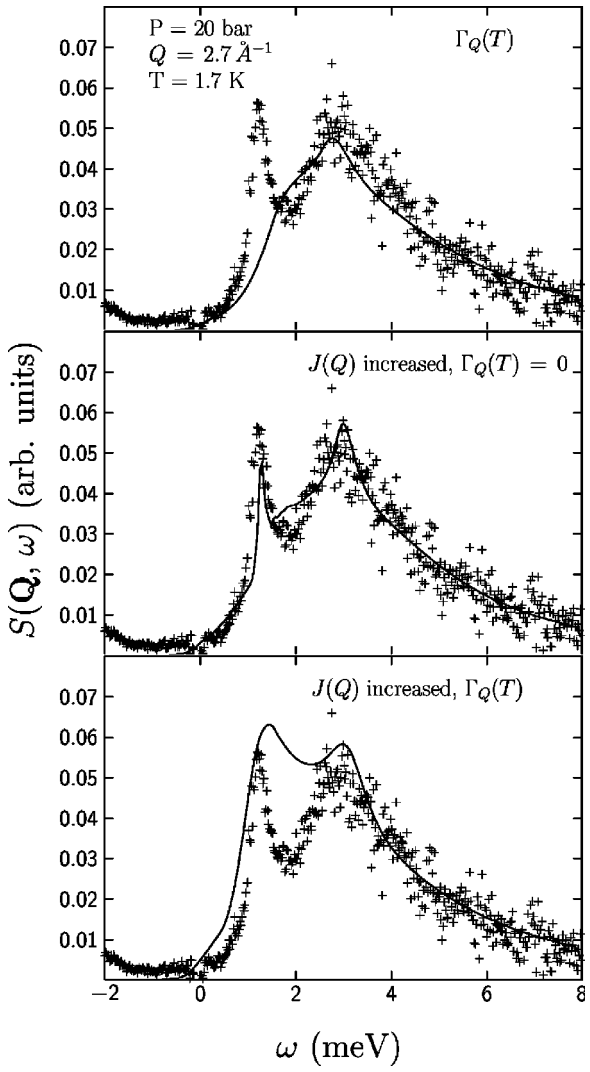

FIG. 13. Dependence of $S(\mathbf{Q},\omega)$ (solid line) at $Q=2.7$ Å^{-1}, $T=1.7$ K, and 20 bar pressure on the magnitude of the three-point interaction, $J(\mathbf{Q})$, compared with experimental data (crosses). Top frame: $S(\mathbf{Q},\omega)$ as in Fig. 9 with $J(\mathbf{Q})$ determined at 0.6 K and held constant with T. Middle frame: $S(\mathbf{Q},\omega)$ calculated with ω_Q^0 having zero width and $J(\mathbf{Q})$ increased by a factor of 1.4 in the real part of the self energy only. Bottom frame: $S(\mathbf{Q},\omega)$ calculated with ω_Q^0 having the observed width and $J(\mathbf{Q})$ increased by a factor of 2 "everywhere."

$\Lambda(Q)$. Second, we investigate the importance of the Bose functions in the zeroth order DS's, Eqs. (27) and (28), and their role in determining the T-dependence of $S(\mathbf{Q},\omega)$. Third, we show how the condensate fraction can be estimated from the data using sum rule arguments.

A. Importance of the vertex Λ

In this section we investigate the importance of the vertex function $\Lambda(Q)$ and the four-point interaction contained in $\chi'_\Lambda(Q)$ on the structure of $S_S(\mathbf{Q},\omega)=-\{[n_B(\omega)+1]/\pi\}\Im m[\Lambda(Q)G(Q)\Lambda(Q)]$. To set the stage, we show in Fig. 14 the singular $S_S(\mathbf{Q},\omega)$ at $Q=3.0$ Å^{-1} and $T=0.6$ K with $\Lambda(Q)$ set to one. Figure 14 shows the basic features of $S_S(\mathbf{Q},\omega)$, a sharp single excitation p-r peak plus a broader resonance in the two p-r excitation band centered at $\omega \approx 4$ meV. While we expect the sharp peak to come from the single particle Green's function, $G(\mathbf{Q},\omega)$, Fig. 14 demonstrates that the broader resonance also comes from $G(\mathbf{Q},\omega)$, from a second resonance in G where the two-excitation density of states is not zero as noted by Fåk and Bossy.[3] The two excitation density of states enters $G(\mathbf{Q},\omega)$ via the self energy Σ^{12} as shown in Eqs. (24)–(26). These two contributions to $S(\mathbf{Q},\omega)$ were found in the early calculations of $G(\mathbf{Q},\omega)$ by Jackson[15] and $\Lambda(Q)=1$ has been used in all recent calculations to date except that of Pistolesi[19] and Szwabinski and Weyrauch.[20]

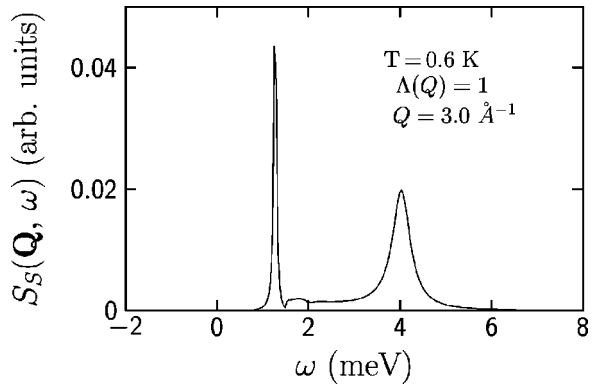

FIG. 14. $S_S(\mathbf{Q},\omega)$ calculated with vertex function set to one $[\Lambda(Q)=1]$ such that $S_S(\mathbf{Q},\omega)=-\{[n_B(\omega)+1]/\pi\}\Im m(G(\mathbf{Q},\omega))$ at $T=0.6$ K and $Q=3.0$ Å^{-1}.

In Fig. 15 we show $S_S(\mathbf{Q},\omega)$ calculated with $\Lambda(Q)\neq 1$ for three different values of the four-point interaction, $I(\mathbf{Q})=0$, 100 and 200 KÅ^3. Figure 16 shows the corresponding values

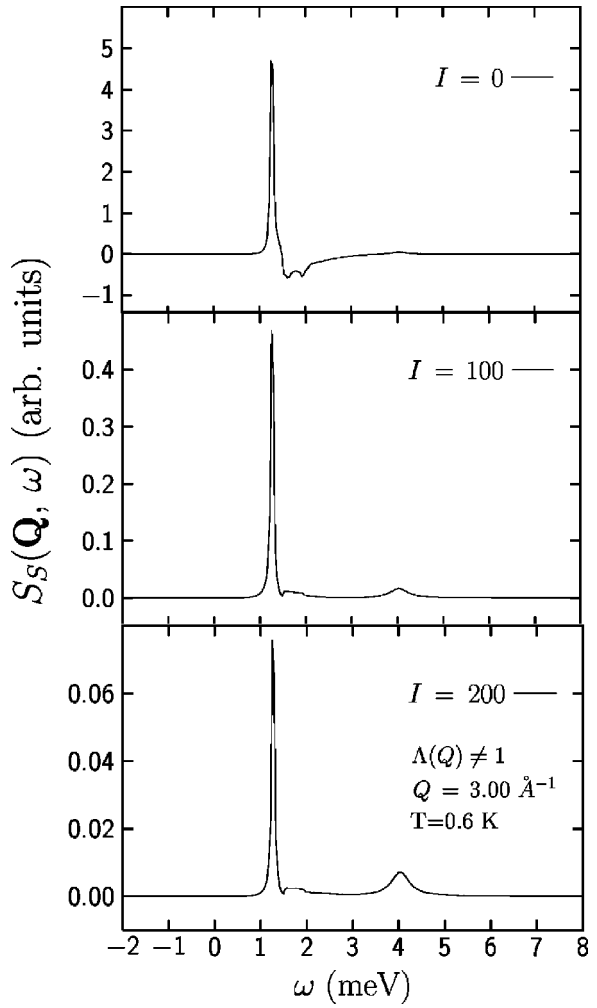

FIG. 15. $S_S(\mathbf{Q},\omega)=\{[n_B(\omega)+1]/\pi\}\Im m(\chi_S(\mathbf{Q},\omega))$ vs ω for $Q=3.0$ Å^{-1}, $T=0.6$ K and three values of the four-point interaction $I(\mathbf{Q})$ in units of KÅ^3. $S_S(\mathbf{Q},\omega)$ is in the same units as Fig. 14.

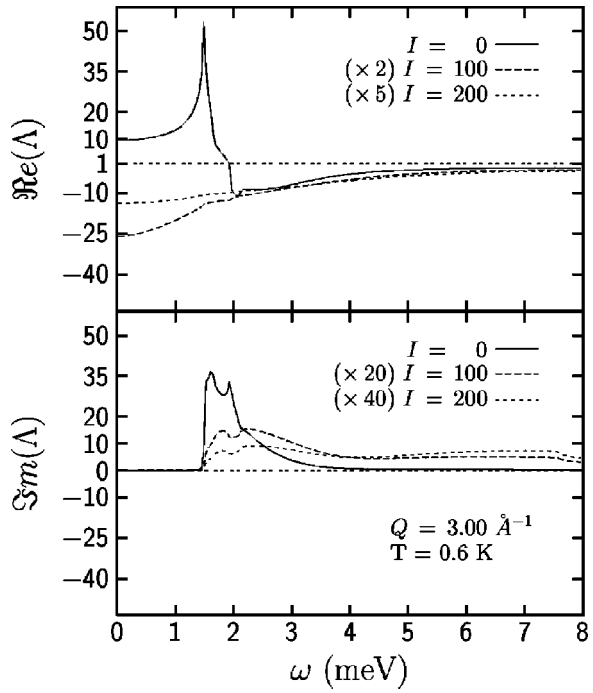

FIG. 16. Real and imaginary parts of the vertex function $\Lambda(Q)$ for $Q=3.0$ Å^{-1}, $T=0.6$ K for three values of the four-point interaction $I(\mathbf{Q})=0$, 100, and 200 in units of KÅ^3. The vertex $\Lambda(Q)$ is unitless. The values of Λ for $I(\mathbf{Q})=100$ and 200 KÅ^3 have been rescaled for clarity. The horizontal line at $\Re e(\Lambda)=1$ serves as a guide to the eye as does $\Im m(\Lambda)=0$.

of the real and imaginary parts of $\Lambda(\mathbf{Q},\omega)$. To discuss $S_S(\mathbf{Q},\omega)$ and $\Lambda(Q)$, we note that $\Lambda(Q)$ in Eq. (16) can be written in the form

$$\Lambda(Q)=\sqrt{n_0}[1+J(\mathbf{Q})\chi'_\Lambda(Q)], \tag{32}$$

where

$$\chi'_\Lambda(Q)=\frac{\chi'^0_\Lambda(Q)}{1-I(\mathbf{Q})\chi'^0_\Lambda(Q)}. \tag{33}$$

The three-point interaction $J(\mathbf{Q})$ in Eq. (32) was held fixed at the value required in Σ^{12} to get the energy of the single p-r mode correct in $G(\mathbf{Q},\omega)$, as discussed in Sec. III. When $I(\mathbf{Q})=0$, $\chi'_\Lambda(Q)$ reduces to the zeroth order DS, $\chi'^0_\Lambda(Q)$. The real part of $\chi'^0(\mathbf{Q},\omega)$ has nearly singular behavior at $\omega\approx 2\Delta$. (Recall that we added a small imaginary part $\eta=5$ μeV to the ω^0_Q in χ'^0.) In this case, $\Re e(\Lambda(\mathbf{Q},\omega))$ becomes very large at energies ω near the single p-r energy at Q values beyond the roton (see the upper frame of Fig. 16). Effectively, the $J(\mathbf{Q})\chi'^0(Q)$ is much larger than the unit term in $\Lambda(Q)$. As a result, the magnitude of the single p-r excitation peak in $S_S(\mathbf{Q},\omega)$ becomes very large (see the upper frame of Fig. 15). For $I(\mathbf{Q})=0$, the weight in the single p-r peak is a factor of 100 greater than that in the "bare" $G(\mathbf{Q},\omega)$ for the parameters used here (compare Fig. 14 and the upper frame of Fig. 15). As $I(\mathbf{Q})$ is increased, the singularity is moderated, the magnitude of $\chi'_\Lambda(Q)$ is decreased and the weight of the single excitation peak in $S_S(\mathbf{Q},\omega)$ is decreased (see Fig. 15). For $I(\mathbf{Q})=200$ KÅ^3, the value used for

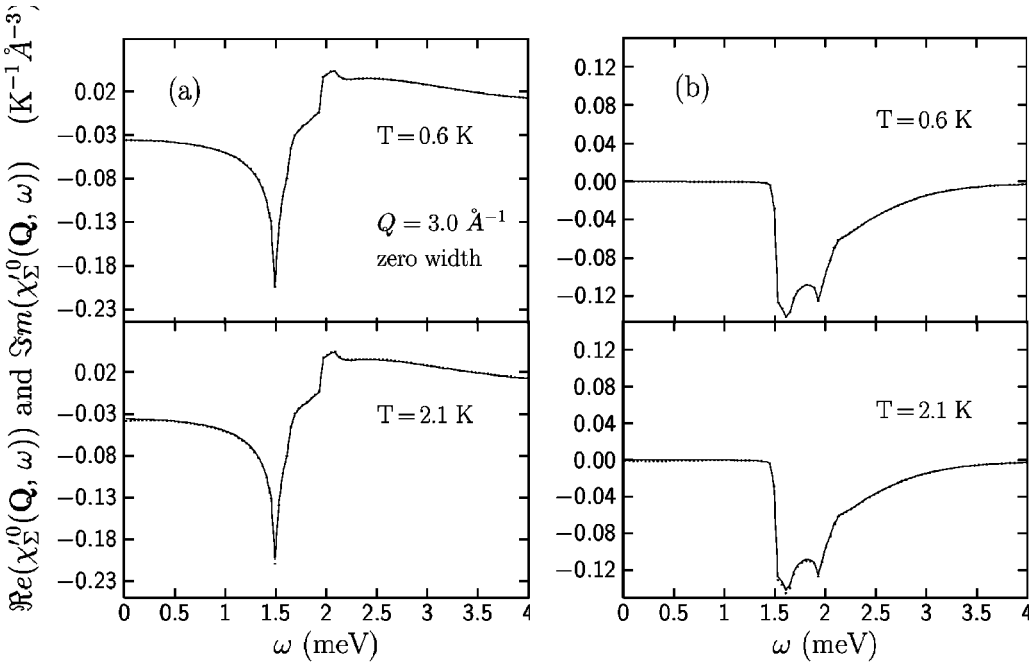

FIG. 17. Real (a) and imaginary (b) parts of $\chi'^0_\Sigma(\mathbf{Q},\omega)$ at $Q=3.0$ Å^{-1} vs ω at temperatures $T=0.6$ K and 2.1 K calculated using p-r energies ω^0_Q having zero width. The dotted line is $\chi'^0_\Sigma(\mathbf{Q},\omega)$ calculated with the Bose factors $n_B(\omega)$ included in $\chi'^0_\Sigma(\mathbf{Q},\omega)$, the solid line without. The two lines are nearly identical.

the results in Sec. III, the weight in the single p-r peak is comparable to that in Fig. 15.

These results show that a finite value of $I(\mathbf{Q})$ is required in $\chi'_\Lambda(Q)$ to get agreement with experiment. Use of the bare $\chi'^0_\Lambda(\mathbf{Q},\omega)$ in $\Lambda(Q)$ which has singular behavior would not give good results. To assess the magnitude of $I(\mathbf{Q})$, we note that the Landau parameter F^s_0 (see Glyde,[22] pp. 247–250), which describes $I(\mathbf{Q})$ in dimensionless units in liquid ^{3}He at $Q\rightarrow 0$, is 52.2 at 20 bar pressure. Dividing F^s_0 by the density of states which is $0.014(\text{KÅ}^3)^{-1}$ gives 3730 KÅ^3. But this value decreases by a factor of 10 as Q increases bringing it in line with values of $I(\mathbf{Q})$ used here. Pistolesi[19] obtains a value of −4.7 meV Å^3 for g_4 which is equivalent to −55 KÅ^3, Bedell *et al.*[16] quote a value of $g_4=-4\times10^{-39}$ erg cm^3 (=−30 KÅ^3) (at a pressure of 24.2 bar and roton pair momentum 2.7 Å^{-1}), and Szwabinski and Weyrauch[20] use $g_4=190$ KÅ^3 in their calculations. Essentially, our value of $I(\mathbf{Q})=200$ KÅ^3 is in excellent agreement with that used by Szwabinski and Weyrauch. Thus a value of $I(\mathbf{Q})\approx 200$ KÅ^3 is a physically reasonable value. A positive $I(\mathbf{Q})$ value indicates that the interactions between the rotons are repulsive at this Q value.

From an operational point of view, the magnitude of $I(\mathbf{Q})$ adjusts the weight in the single excitation peak relative to that in the broad resonance at $\omega\approx 4$meV in the two-excitation band. Approximately, for large $I(\mathbf{Q})$, $\chi'_\Lambda(Q)\approx -1/I(\mathbf{Q})$. Typical values of $J(\mathbf{Q})$ used here are $J(\mathbf{Q})=700$ KÅ^3. While this is larger than the four-point vertex $I(\mathbf{Q})$, it is comparable to other interactions found in quantum liquids. Szwabinski and Weyrauch[20] quote a value of $g_3=0.3$ K nm$^{3/2}$ which when converted to units of KÅ^3 and divided by the square roots of both the density of liquid ^{4}He, $n=0.022$ Å^{-3}, and the condensate fraction, $\sqrt{n_0}$, yields $J(\mathbf{Q})=g_3/\sqrt{n_0 n}=240$ KÅ^3. Juge and Griffin[18] quote a value of $g_3=1.9\times10^{-39}$ erg cm^3 Å$^{-3/2}$ for a wave vector $Q=2.8$ Å^{-1} and $T=1.2$ K, corresponding to $J(\mathbf{Q})=350$ KÅ^3. Our value of $J(\mathbf{Q})$ is of the same order of magnitude as theirs but it is determined explicitly from the self energy.

B. Importance of the Bose functions $n_B(\omega)$ in the dynamic susceptibilities

The zeroth order DS's used in the present calculations given by Eqs. (27) and (28) have four terms. The first term is the only term that survives at $T=0$ K for positive energies, $\omega>0$. All previous calculations in liquid ^{4}He have retained only the first term. In calculations of $S(\mathbf{Q},\omega)$ in anharmonic solids, all four terms are usually included. We kept all four terms to test whether the thermal terms proportional to the Bose functions could play a role in the temperature dependence of $S(\mathbf{Q},\omega)$. Particlularly, $S(\mathbf{Q},\omega)$ increases in intensity at low ω with increasing temperature which could arise from the thermal terms in $\chi'^0(\mathbf{Q},\omega)$.

Figures 17(a) and 17(b) show the real and imaginary parts of $\chi'^0_\Sigma(\mathbf{Q},\omega)$ calculated using temperature independent p-r energies that have zero width. For temperatures between $T=0.6$ K and $T=2.1$ K, $\chi'^0_\Sigma(\mathbf{Q},\omega)$ is essentially independent of T. Thus the finite temperature terms of $\chi'^0_\Sigma(\mathbf{Q},\omega)$ make an insignificant contribution, except at very low energies, $\omega<kT$, and can be neglected.

Figures 18(a) and 18(b) show $\chi'^0_\Sigma(\mathbf{Q},\omega)$ using p-r energies, $\omega^0_Q+i\Gamma_Q(T)$, where ω^0_Q is again independent of T and $\Gamma_Q(T)$ are the observed half widths. In this case $\chi'^0_\Sigma(\mathbf{Q},\omega)$ has a very significant temperature dependence. The tempera-

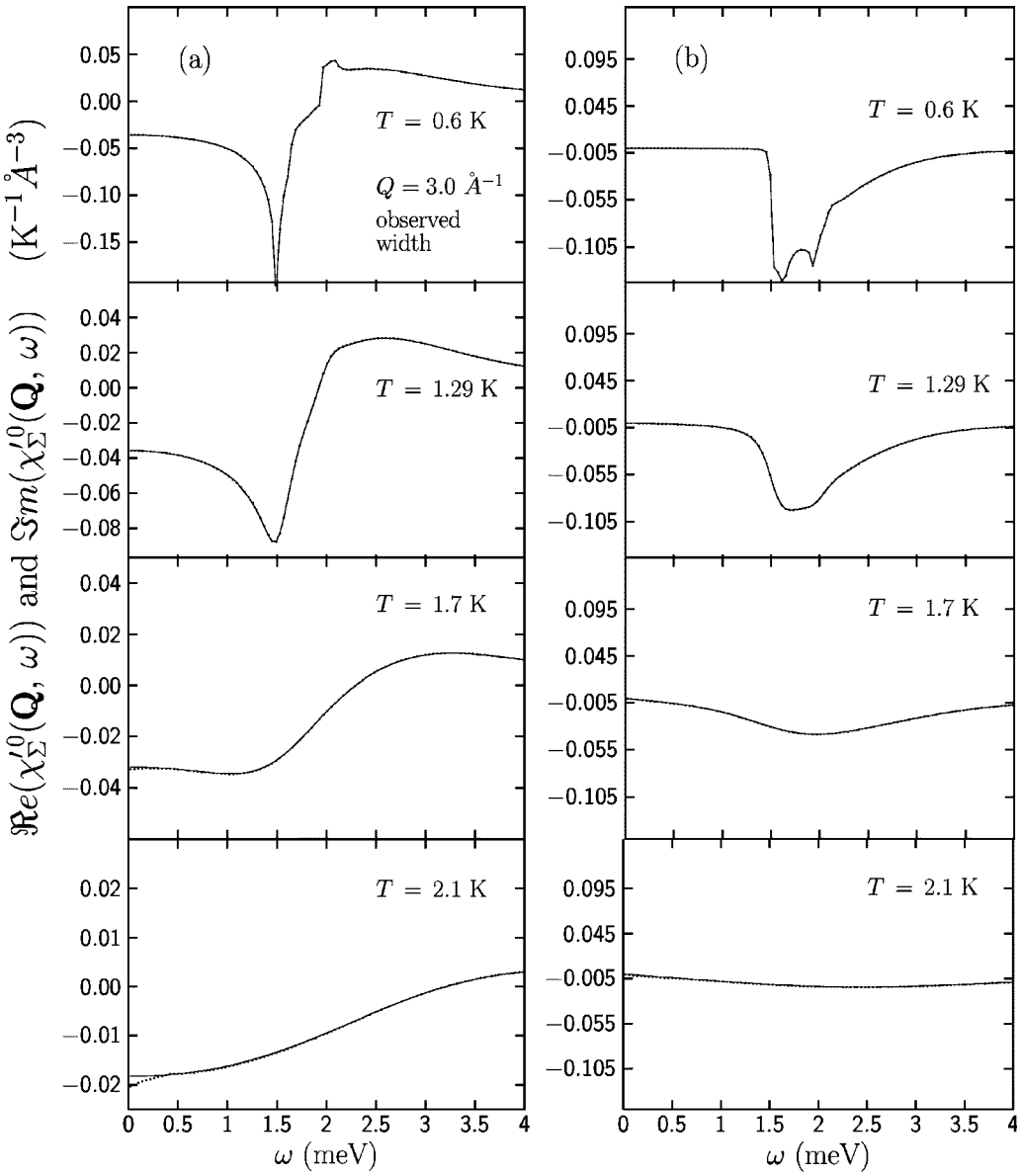

FIG. 18. The same as in Fig. 17, but using $\omega_Q^0 + i\Gamma_Q$ with the observed width Γ_Q.

ture dependence of $\chi'^0_\Sigma(\mathbf{Q},\omega)$ arises from the T dependence of $\Gamma_Q(T)$ in the first term of $\chi'^0_\Sigma(\mathbf{Q},\omega)$ and not from the terms in $\chi'^0_\Sigma(\mathbf{Q},\omega)$ containing the Bose functions. The temperature dependence of the model $S(\mathbf{Q},\omega)$ at low ω shown in Figs. 9 and 10 arises from the temperature dependence of $\Gamma_Q(T)$ in $\chi'^0_R(\mathbf{Q},\omega)$ not from the "thermal" terms of $\chi'^0_R(\mathbf{Q},\omega)$.

C. Condensate fraction and *f*-sum rule

The total dynamic structure factor satisfies the f-sum rule,

$$\frac{1}{\omega_R} f \equiv \frac{1}{\omega_R} \int d\omega S(\mathbf{Q},\omega)\omega = 1, \tag{34}$$

where $\omega_R = \hbar Q^2/2m$ is the free atom recoil frequency. The separate contributions from the singular and regular parts, $S(\mathbf{Q},\omega) = S_S(\mathbf{Q},\omega) + S_R(\mathbf{Q},\omega)$, to the f-sum rule have also been determined.[25] The contribution from the singular part is

$$\frac{1}{\omega_R} f_S = \frac{1}{\omega_R} \int d\omega S_S(\mathbf{Q},\omega)\omega = n_0\left(1 - \frac{h_Q}{\omega_R}\right), \tag{35}$$

where n_0 is the condensate fraction and h_Q is a potential energy term that is difficult to evaluate directly. However, h_Q is approximately independent of Q so that h_Q/ω_R should be small at high Q. Indeed, it is this contribution to $S(\mathbf{Q},\omega)$ that is used[5] at very high Q values (25–100 Å^{-1}) to determine $n_0(T)$.

Assuming that h_Q/ω_R is small (negligible) we may estimate n_0 using $f_S/\omega_R = n_0$ at low T from the model $S_S(\mathbf{Q},\omega)$ and data considered here. Attributing the sharp peak and the broad resonance at $\omega \approx 3.5$ meV to $S_S(\mathbf{Q},\omega)$, as we have done throughout, we may calculate f_S/ω_R numerically from the data or from the model. The two give similar values. In this way we find at low T

$$f_S/\omega_R = n_0 = 0.068 \pm 0.07, \quad \text{at SVP;}$$

and

$$f_S/\omega_R = n_0 = 0.036 \pm 0.05, \quad \text{at 20 bars;} \tag{36}$$

using data at $Q=2.65$ Å^{-1} and at $Q=3.0$ Å^{-1}, respectively. The SVP value is in good agreement with an accurate direct measurement[5] giving $n_0=(7.25\pm0.75)\%$ at low T. The 20 bar value is consistent with Monte Carlo calculations.[26] Thus data and models of $S(\mathbf{Q},\omega)$ at intermediate Q values "beyond the roton" can be used to estimate n_0 using sum-rule arguments. In systems where there are no direct measurements of the condensate, this method may be used to find approximate values of $n_0(T)$.

V. DISCUSSION

In this study we have formally separated the DS of a Bose fluid into a singular and regular part, $\chi(\mathbf{Q},\omega)=\chi_S(\mathbf{Q},\omega)+\chi'_R(\mathbf{Q},\omega)$. The χ_S is proportional to the condensate fraction $n_0(T)$ and the single particle Green's function, $G(\mathbf{Q},\omega)$, as seen from Eq. (4) and (6). $\chi'_R(\mathbf{Q},\omega)$ involves states above the condensate only. A key property of a Bose fluid with BEC is that the total $\chi(\mathbf{Q},\omega)$ and $G(\mathbf{Q},\omega)$ have common poles. Thus the density response (χ) and the single particle response (G) have a common characteristic excitation energy dispersion curve. In superfluid ^{4}He below T_c where there is a condensate, this common energy dispersion curve is the p-r energy dispersion curve. Particularly, in superfluid ^{4}He, there are no low energy, single particle excitations lying under the p-r curve to which the p-r mode can decay since the mode of G is part of the p-r mode itself. Thus the p-r excitations can decay only to themselves and this four "phonon" process is very small at low temperature. In this way the well defined p-r mode in superfluid ^{4}He arises because there is a condensate. In normal ^{4}He where there is no BEC, there is no p-r mode except in the long wave limit.

At low Q and ω, and low temperature, all of the weight of $S(\mathbf{Q},\omega)$ lies in the single common pole—i.e., $S(\mathbf{Q},\omega)=S(\mathbf{Q})\delta(\omega-\omega_\mathbf{Q})$. In this case the separation of χ into χ_S and χ_R is not very useful. Similarly, in the roton region ($Q\approx1.95$ Å^{-1}), where ω_Q is again low, almost all of $S(\mathbf{Q},\omega)$ lies in a single peak. Again, χ_S and χ_R must contribute in the same energy range and the separation of χ into χ_S and χ_R is not very useful.

At higher wave vectors ($Q\geqslant2.5$ Å^{-1}), $S(\mathbf{Q},\omega)$ peaks at higher energy, the weight in the p-r peak is much smaller and $S(\mathbf{Q},\omega)$ has substantial weight at energies above ω_Q. The $S(\mathbf{Q},\omega)$ is spread over a wide energy range and there is more opportunity to identify the components $\chi_S(\mathbf{Q},\omega)$ and $\chi'_R(\mathbf{Q},\omega)$ within the total. Specifically, in the present model at these wave vectors, the sharp peak in $\chi(\mathbf{Q},\omega)$ arises from the sharp peak in $G(\mathbf{Q},\omega)$ in $\chi_S(\mathbf{Q},\omega)$. The weight of the sharp peak is proportional to $n_0(T)$ and the sharp peak disappears completely from $\chi(\mathbf{Q},\omega)$ in the normal phase where $n_0(T)=0$. This basic temperature dependence arising from $n_0(T)$ which reproduces experiment is the chief finding here. The value of n_0 at low T can be estimated from this structure. We also found that the increase in intensity at low ω with increasing temperature arises from the thermal broadening of the p-r modes. We would not expect the present model to describe the T dependence of $S(\mathbf{Q},\omega)$ at the phonon or roton Q well since the coupling between χ_S and χ_R is strong at low ω. Also, there is a mode in $\chi_R(\mathbf{Q},\omega)$ at phonon wavevectors Q since there is a sound mode in normal ^{4}He. We have assumed here, at $Q\gtrsim2.5$ Å^{-1}, that there is no mode in χ_R.

As Q increases, the weight in the sharp peak decreases. At $Q\geqslant3.6$ Å^{-1}, the weight in the sharp peak is not observable and the p-r mode is said to end. All the intensity arising from $\chi_S(\mathbf{Q},\omega)$ at $Q\geqslant3.6$ Å^{-1}, which is proportional to $n_0(T)$, now lies at higher energy, $\omega\geqslant2\Delta$, as a broad peak in the multi-excitation band. This broad resonance gradually sharpens with a further increase in Q until at very high Q (e.g., $Q\simeq25$ Å^{-1}) it is a "delta function" peak at the free atom recoil energy, $\omega_R=\hbar Q^2/2m$. Thus the broad resonance at intermediate Q evolves into the peak that is used to determine the condensate fraction in very high momentum transfer experiments.[5]

$\chi(\mathbf{Q},\omega)$ in anharmonic solids can be written in the same form as the model used here. If we write $\chi(\mathbf{Q},\omega)$ as the sum of one phonon scattering $(\chi_1(\mathbf{Q},\omega))$, two phonon scattering $(\chi_2(\mathbf{Q},\omega))$, interference between the one and two phonon scattering $(\chi_{12}(\mathbf{Q},\omega))$ plus the remainder, we have

$$\begin{aligned}\chi(\mathbf{Q},\omega) &= \chi_1(\mathbf{Q},\omega)+\chi_{12}(\mathbf{Q},\omega)+\chi_{21}(\mathbf{Q},\omega)+\chi_2(\mathbf{Q},\omega)\cdots,\\ &= \Lambda G\Lambda+\chi_R,\end{aligned} \tag{37}$$

where $\Lambda G\Lambda=\chi_1+\chi_{12}+\chi_{21}$ has the same structure as Eq. (4). G is the single phonon Green's function and $\chi'^0(\mathbf{Q},\omega)$ in Λ is the two phonon DS. The cubic anharmonic term plays the role of J and $I=0$. A comparison of the magnitude of the interference terms in liquid and solid helium has been made.[22]

In liquid ^{4}He at $p\geqslant20$ bars, $S(\mathbf{Q},\omega)$ at the "maxon" displays the same physics as $S(\mathbf{Q},\omega)$ at Q values "beyond the roton" considered here. For example, at 20 bars the "maxon" energy given by the position of the sharp peak in $S(\mathbf{Q},\omega)$, $\omega_Q=1.283$ meV is right at the limit of $2\Delta(\Delta=0.6355$ meV). Thus, as at higher pressure, the p-r energy at the maxon is limited by the requirement $\omega_Q\leqslant2\Delta$. The weight in the sharp p-r peak at 20 bar is much less than that at SVP. The weight of $S(\mathbf{Q},\omega)$ above 2Δ at 20 bar is much greater than that at SVP. Thus as pressure is increased[27] and ω_Q moves toward 2Δ, weight is transferred from the sharp "p-r" peak to the broad peak that lies above 2Δ in the two excitation band. As temperature is increased, the weight in the sharp "p-r" peak at the maxon decreases uniformly with increasing T and the maxon energy is nearly constant independent of T as seen at Q values "beyond the roton." The maxon energy actually decreases marginally with increasing T. Thus the maxon at 20 bar could be described by the present model.

The reason that ω_Q is largely independent of T when ω_Q is right at the limit, $\omega_Q\simeq2\Delta$, is probably a combination of factors. First, the roton energy $\Delta(T)$ decreases with increasing T. If ω_Q cannot exceed 2Δ, then we would expect the position of the sharp peak to decrease with T as 2Δ decreases with T, or to disappear. However, the singularity that pre-

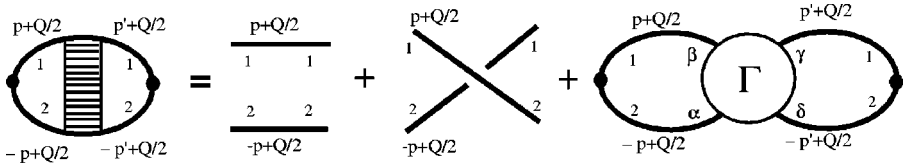

FIG. 19. Diagrammatic representation of Eq. (A8) for $\chi(p,p';Q)$.

$$\chi \quad = \quad \chi^0 \quad + \quad \chi^0 \quad \Gamma \quad \chi^0$$

vents any sharp component from having an energy greater than 2Δ also softens with increasing T as the p-r excitations broaden. The softening of the edge of the two-excitation band DOS is seen in Fig. 18(b), for example, when the observed width of the p-r modes is included in the calculation of χ'^0_Σ. This softening would reduce the amount ω_Q must decrease with T to follow $2\Delta(T)$. Third, the repulsion between the single and pair excitation scattering which keeps ω_Q below 2Δ also weakens with increasing T, as $n_0(T)$ decreases. In the present model, we allowed $n_0(T)$ to decrease with increasing T. We have not allowed the p-r energies to decrease with increasing T. Clearly, getting the temperature dependence of $S(\mathbf{Q},\omega)$ completely correct at $\omega \simeq 2\Delta$ would require an accurate model including the temperature dependence of the $\omega_Q(T)$, $\Gamma_Q(T)$ and $n_0(T)$.

To compare with recent calculations, we note that Juge and Griffin[18] have evaluated the single (G) and pair (χ) p-r response functions using several models for ω_Q^0 and including temperature dependent widths Γ_Q. Their results show how G and χ depend on the model assumptions for ω_Q^0, $g_3 = \sqrt{n_0 n} J$ and $g_4 = I$. They note particularly that the coupling of G and χ via g_3 vanishes at T_λ where $n_0 = 0$ as in the present formulation.

In a direct comparison with their data for $S(\mathbf{Q},\omega)$, Fåk and Bossy[3] begin with the Gavoret and Nozières expression, Eq. (4), and set $\Lambda = 1$ so that $\chi = Z_1 G(\mathbf{Q},\omega) + \chi_R(\mathbf{Q},\omega)$. Their $G(\mathbf{Q},\omega)$ is Eq. (3) with a weight Z_1. The ω_Q^0 is a FC like single p-r energy which we have adopted here. χ_R is represented by a DHO function as in model A here. The Z_1, the g_3 in Σ[12], and the DHO are obtained by fits to data. Their g_3 is somewhat smaller, but comparable to that found here. To represent the T-dependence of χ, they take $Z_1 \propto n_0(T)$ and χ_R is refitted at each T. This provides a good fit to data suggesting that Z_1 is indeed approximately proportional to $n_0(T)$. The two peaks in $S(\mathbf{Q},\omega)$ arise from $G(\mathbf{Q},\omega)$. $\chi_R(\mathbf{Q},\omega)$ is largely independent of T, especially at high ω.

Pistolesi has created a model in which the neutrons excite either single (G) or pairs (χ_2) of p-r excitations at $T = 0$ K. The single and pair processes interact via $g_3(\mathbf{Q})$. The total χ is structurally the same as the first term of Eq.(4) plus a two p-r term χ_2. The G is given by Eq. (3). The χ_2 is written as $\chi_2 = \tilde{\chi}/(1 - I_{12}\tilde{\chi})$ where $I_{12} = g_3 G g_3$. $\tilde{\chi}(\tilde{G})$ includes all interactions except I_{12}. This formulation has the virtue that all terms clearly have a common denominator $(1 - g_3 \tilde{G} g_3 \tilde{\chi})$ as required by the dielectric formulation. The χ is, however, fitted to all of the intensity including that of high ω. This cannot be appropriate since most of the intensity at $\omega > 2\Delta$ is independent of T and exists, unchanged, in normal ^{4}He where there are no p-r excitations. The fit to data shows that ω_Q does not exceed 2Δ.

Szwabinski and Weyrauch have evaluated the Gavoret and Nozières expression for liquid ^{4}He at $T = 0$ K. This formulation is essentially a $T = 0$ K version of the present expressions. They were more ambitious in that the single p-r Green's function and ω_Q were obtained by an iteration process so that the single G in Eq. (26) and the G used (χ^0) in Eq. (27) were the same and internally consistent. They show fits to data having both positive and negative $g_4(\mathbf{Q})(=I(\mathbf{Q}))$ values. They found $g_3(\mathbf{Q})(\Rightarrow J(\mathbf{Q}))$ larger than g_4 as found here.

ACKNOWLEDGMENTS

It is a pleasure to acknowledge valuable discussions with P. Nozières, B. Fåk, J. Bossy, J. Szwabinski, and M. Weyrauch. The authors are particularly grateful to B. Fåk for a critical reading of the manuscript. Partial support from the National Science Foundation, DMR-0115663, is gratefully acknowledged.

APPENDIX: THE DYNAMIC SUSCEPTIBILITY

In this section, we separate the DS, $\chi(\mathbf{Q},\omega)$, into a part involving the condensate [the zero momentum state ($p = 0$)],

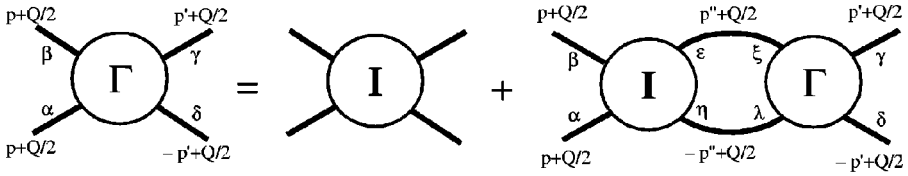

FIG. 20. Diagrammatic representation of Eq. (A12) for $\Gamma(p,p';Q)$.

$$\Gamma \quad = \quad I \quad + \quad I \quad \chi^0 \quad \Gamma$$

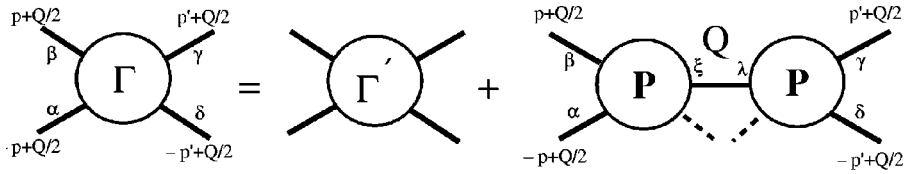

FIG. 21. Diagrammatic representation of Eq. (A20) for $\Gamma(p,p';Q)$.

$$\Gamma \quad = \quad \Gamma' \quad + \quad P \quad G \quad P$$

$\chi_S(\mathbf{Q},\omega)$, and a part that contains states above the condensate ($p \neq 0$) only, $\chi'_R(\mathbf{Q},\omega)$,

$$\chi(\mathbf{Q},\omega) = \chi_S(\mathbf{Q},\omega) + \chi'_R(\mathbf{Q},\omega). \tag{A1}$$

This is done essentially by expanding $\chi(\mathbf{Q},\omega)$ in momentum states, identifying the terms involving $p=0$, and collecting all these terms in $\chi_S(\mathbf{Q},\omega)$. The separation for χ is formally the same as is done often for the Hamiltonian in Bose systems (Bogoliubov,[28] Hugenholtz and Pines,[29] Mahan[30]) to identify the terms that depend on the condensate ($p=0$). Our formulation is identical to that of Gavoret and Nozières except that it is done here at finite temperature, T.

We begin with the DS for the density response of a Bose fluid as

$$\chi(\mathbf{Q},\tau) = -\frac{1}{N}\langle T_\tau\, \rho(\mathbf{Q},\tau)\rho^\dagger(\mathbf{Q},0)\rangle, \tag{A2}$$

where $\rho(\mathbf{Q})=\Sigma_k\, a_k^\dagger a_{k+Q}=\Sigma_p\, a_{p-Q/2}^\dagger a_{p+Q/2}$ is the Fourier transform of the number density in a second quantized representation. The a_p and $a_p^\dagger$ are the usual operators that annihilate and create particles in momentum state $\hbar p$, $\tau=it/\hbar$ is an imaginary time, T_τ is the time ordering operator and N is the number of Bosons. The dynamic structure factor $S(\mathbf{Q},\omega)$ is related to $\chi(\mathbf{Q},\omega)$ by

$$S(\mathbf{Q},\omega) = -\frac{1}{\pi}[n_B(\omega)+1]\Im m(\chi(\mathbf{Q},\omega+i\eta)), \tag{A3}$$

where $\chi(\mathbf{Q},\omega+i\eta)=\chi(\mathbf{Q},i\omega_n)$ is the Fourier transform of Eq. (A2) defined at the frequency points $i\omega_n$, $\omega+i\eta$ is the usual continuation of $i\omega_n$ to the real axis and $n_B(\omega)=(e^{\beta\omega}-1)^{-1}$ is the Bose function with $\beta=(k_BT)^{-1}$.

The corresponding single particle Green's functions for the Bose fluid having a condensate are

$$G_{\alpha\beta}(\mathbf{p},\tau) = -\langle T_\tau\, a_p^\alpha(\tau)a_p^{\dagger\beta}(0)\rangle, \tag{A4}$$

where $\alpha=1,2$. For $\alpha=1$, $a_p^\alpha=a_p$ and $\alpha=2$, $a_p^\alpha=a_{-p}^\dagger$. $G_{11}(\mathbf{p},\tau)$ is the usual Green's function describing propagation of particles and the others (e.g., G_{12}) are anomalous functions which are not zero if there is a condensate.

Inserting the expression for $\rho(\mathbf{Q})$ into Eq. (A2), we have

$$\chi(\mathbf{Q},\tau) = \frac{1}{NV}\sum_{p,p'}\chi(p,p';\mathbf{Q},\tau), \tag{A5}$$

where

$$\chi(p,p';\mathbf{Q},\tau) \equiv V\langle T_\tau\, a_{p-Q/2}^\dagger(\tau)a_{p+Q/2}(\tau)a_{p+Q/2}^\dagger(0)a_{p-Q/2}(0)\rangle. \tag{A6}$$

Our starting point is the equation for the two-body Green's function,

$$G_{\alpha\beta\gamma\delta}(1,2;3,4) = V\langle a_{p_1}^\alpha(\tau_1)a_{p_2}^\beta(\tau_2)a_{p_3}^\gamma(\tau_3)a_{p_4}^\delta(\tau_4)\rangle, \tag{A7}$$

given, for example, by Abrikosov *et al.*[31] (1963) on p. 139. We note that $\chi(p,p';\mathbf{Q},\tau)=G_{2112}(-p+Q/2,p+Q/2;p'+Q/2,-p'+Q/2)$. That is, χ and $G_{\alpha\beta\gamma\delta}$ are the same if $p_1=-p+Q/2$ and $\alpha=2$, $p_2=p+Q/2$ and $\beta=1$, $p_3=p+Q/2$ and $\gamma=1$, $p_4=-p'+Q/2$ and $\delta=2$, $\tau_1=\tau_2=\tau$ and $\tau_3=\tau_4=0$. From the equation for the Fourier transform of Eq. (A7) we obtain the equation for the Fourier transform of $\chi(p,p';\mathbf{Q},\tau)$,

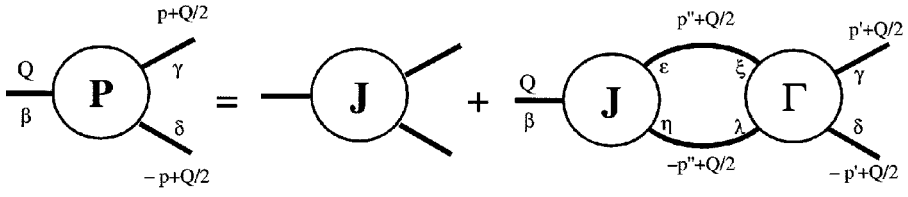

FIG. 22. Diagrammatic representation of Eq. (A26) for $P(p,Q)$.

$$P \quad = \quad J \quad + \quad J \quad \chi'_0 \quad \Gamma$$

$$\chi(p,p';Q) = [\chi^0_{2112}(p,Q)\delta_{\mathbf{p}',-\mathbf{p}} + \chi^0_{2211}(p,Q)\delta_{\mathbf{p}',\mathbf{p}}] \times V(-\beta\hbar)\delta_{n,n'} + \chi^0_{2\alpha1\beta}(p,Q)\Gamma_{\alpha\beta\gamma\delta}(p,p';Q)\chi^0_{\gamma1\delta2}(p',Q), \tag{A8}$$

where

$$\chi^0_{\alpha\beta\gamma\delta} \equiv G_{\alpha\beta}\left(-p+\frac{Q}{2}\right)G_{\gamma\delta}\left(p+\frac{Q}{2}\right) \tag{A9}$$

represents the independent propagation of a pair of particles and

$$\chi(Q) = \frac{V}{N}\int d\overline{p}\int d\overline{p'}\,\chi(p,p';Q), \tag{A10}$$

where

$$\int d\overline{p} = \frac{1}{V}\sum_{\mathbf{p}}\left(-\frac{1}{\beta\hbar}\right)\sum_n, \tag{A11}$$

and $G(p)=G(\mathbf{p},i\omega_{n_p})$, $G(p+Q)=G(\mathbf{p}+\mathbf{Q},i\omega_{n_p}+i\omega_n)$, $Q=\mathbf{Q},i\omega_{n_p}$, $p=\mathbf{p},i\omega_{n_p}$. In Eq. (A8) $\Gamma_{\alpha\beta\gamma\delta}(p,p';Q)$ is the full interaction between a pair of particles and can be written as

$$\Gamma_{\alpha\beta\gamma\delta}(p,p';Q) = I_{\alpha\beta\gamma\delta}(p,p';Q) + I_{\alpha\beta\epsilon\eta}(p,p'',Q)\chi^0_{\epsilon\eta\xi\lambda}(p'',Q)\Gamma_{\xi\lambda\gamma\delta}(p'',p';Q). \tag{A12}$$

In Eq. (A12), $I_{\alpha\beta\gamma\delta}$ represents that part of $\Gamma_{\alpha\beta\gamma\delta}$ which does not have a free pair (χ^0) as an intermediate state. Equations (A8) and (A12) are represented in Figs. 19 and 20, respectively, and are the starting point of our analysis.

Our goal now is to identify the terms in $\chi(Q)$ involving the condensate ($p=0$). We do this exactly as in the case of the Hamiltonian (Bogoliubov [28]) by identifying where $p=0$ and replacing $a_0=a_{-0}=a_0^\dagger$ by $\sqrt{N_0}$. When $p=0$ the Green's function reduces to

$$G_{\alpha\beta}(\mathbf{p},\tau) = -\langle T_\tau\, a_p^\alpha(\tau)a_p^{\dagger\beta}(0)\rangle = -N_0 \tag{A13}$$

for all α, β and the Fourier transform is

$$G_{\alpha\beta}(\mathbf{p},i\omega_n) = \int_0^{\beta\hbar} d\tau e^{i\omega_n\tau}G_{\alpha\beta}(\mathbf{p},\tau), = -N_0\beta\hbar\,\delta_{n,0}. \tag{A14}$$

Using this result, the terms involving the condensate in the free two particle propagator Eq. (A9) can be identified as

$$\chi^0_{\alpha\beta\gamma\delta}(p,Q) = (-N_0\beta\hbar)\delta_{n,0}[G_{\alpha\beta}(Q)\delta_{p,-Q/2} + G_{\gamma\delta}(Q)\delta_{p,Q/2}] + \chi^{0\prime}_{\alpha\beta\gamma\delta}(p,Q), \tag{A15}$$

where $\chi^{0\prime}_{\alpha\beta\gamma\delta}(p,Q)$ involve states above the condensate only. We write Eq. (A15) schematically as

$$\chi_0 = N_0G + \chi_0'. \tag{A16}$$

Explicitly, the zeroth order terms of $\chi_S(\mathbf{Q},\omega)$ [obtained from the first two terms of Eq. (A8)] are

$$\chi_0(\mathbf{Q},\omega) = \frac{N_0}{N}\sum_{\alpha\beta}G_{\alpha\beta}(\mathbf{Q},\omega) + \chi'_{0R}(\mathbf{Q},\omega), \tag{A17}$$

where $n_0=N_0/N$ is the condensate fraction, and

$$\chi'_{0R}(\mathbf{Q},\omega) = \frac{1}{N}\sum_{\mathbf{p}}\left(-\frac{1}{\beta\hbar}\right)\sum_n[\chi^{0\prime}_{2112}(p,Q) + \chi^{0\prime}_{2211}(p,Q)]. \tag{A18}$$

To display how χ_S and χ_R are obtained from Eq. (A8), we write Eq. (A8) schematically, using Eq. (A16), as

$$\chi = (N_0G+\chi_0')+(N_0G+\chi_0')\Gamma(N_0G+\chi_0') = N_0G + N_0G\Gamma\chi_0' + N_0\chi_0'\Gamma G + \chi_0' + \chi_0'\Gamma\chi_0. \tag{A19}$$

We also write Eq. (A12) schematically using Eq. (A16)

$$\Gamma = I + I(N_0G+\chi_0')\Gamma, = \Gamma' + N_0PGP. \tag{A20}$$

All terms involving more than one G vanish (the interaction is zero in these equations). In Eq. (A20),

$$P_{\alpha\beta\gamma}(p',Q) \equiv \Gamma_{\alpha\alpha\beta\gamma}(0,p';Q) \tag{A21}$$

is the four-point interaction with one index zero so that it becomes a three-point interaction. The Γ' is the full four-point interaction given by Eq. (A12) but with χ_0 replaced by χ_0'. Equation (A20) is depicted in Fig. 21.

Substituting Eq. (A20) into Eq. (A19) the full dynamic $\chi(Q)$ in Eq. (A10) is

$$\chi(Q) = \Lambda_\alpha(Q)G_{\alpha\beta}(Q)_\beta\Lambda(Q) + \chi'_R(Q), \tag{A22}$$

where $G_{\alpha\beta}(Q)=G_{\alpha\beta}(\mathbf{Q},i\omega_n)$,

$$_\beta\Lambda(Q) = \sqrt{n_0}\left[1+\int d\overline{p}L_{\beta12}(p,Q)\right], \tag{A23}$$

and

$$\int d\overline{p}L_{\beta12}(p,Q) = \int d\overline{p}P_{\beta\gamma\delta}(p,Q)\chi'^0_{\gamma1\delta2}(p,Q) = \frac{1}{V}\sum_p\left(-\frac{1}{\beta\hbar}\right)\times\sum_n P_{\beta\gamma\delta}(p,Q)G_{\gamma1}\left(p+\frac{Q}{2}\right)\times G_{\delta2}\left(-p+\frac{Q}{2}\right). \tag{A24}$$

The

$$\chi'_R(Q) = \chi'_{0R} + \chi_0'\Gamma'\chi_0' \tag{A25}$$

involves states above the condensate only. That is, $\chi'_R(Q)$ is given exactly by Eqs. (A8) and (A10) in which $\chi'^0_{\alpha\beta\gamma\delta}$ and $\Gamma'_{\alpha\beta\gamma\delta}$ involve states above the condensate only.

We note that P satisfies an equation analogous to Eq. (A12) (see Fig. 22),

$$P = J + J\chi_0'\Gamma',$$

$$= J + \Gamma' \chi_0' J, \tag{A26}$$

and $\chi_0' P = \chi_0' J + \chi_0' \Gamma' \chi_0' J = \chi' J$, where

$$\chi' \equiv \chi_0' + \chi_0' \Gamma' \chi_0 = \chi_0' + \chi_0' I \chi', \tag{A27}$$

for any set of indices $\alpha\beta\gamma\delta$. Thus we may write

$$L_{\beta 12}(p,Q) = P_{\beta\gamma\delta}(p,Q)\chi'^{0}_{\gamma 1\delta 2}(p,Q),$$

$$= J_{\beta\gamma\delta}(p,Q)\chi'_{\gamma 1\delta 2}(p,Q), \tag{A28}$$

and $\chi'_{\gamma 1\delta 2}(p,Q)$ is given by Eq. (A27) and χ_0' by Eq. (A9). Equations (A22), (A23), (A28), and (A25) are the starting points of our model for $\chi(Q)$.

[1] P. Pitaevskii, Sov. Phys. JETP **9**, 830 (1959).
[2] B. Fåk, L. P. Regnault, and J. Bossy, J. Low Temp. Phys. **89**, 345 (1992).
[3] B. Fåk and J. Bossy, J. Low Temp. Phys. **113**, 531 (1998); **112**, 1 (1998).
[4] J. Gavoret and P. Nozières, Ann. Phys. (N.Y.) **28**, 349 (1964).
[5] H. R. Glyde, R. T. Azuah, and W. G. Stirling, Phys. Rev. B **62**, 14 337 (2000).
[6] R. A. Cowley and A. D. B. Woods, Can. J. Phys. **49**, 177 (1971).
[7] A. D. B. Woods and R. A. Cowley, Rep. Prog. Phys. **36**, 1135 (1973).
[8] A. J. Smith, R. A. Cowley, A. D. B. Woods, W. G. Stirling, and P. Martel, J. Phys. C **10**, 543 (1977).
[9] B. Fåk and K. H. Andersen, Phys. Lett. A **160**, 468 (1991).
[10] H. R. Glyde, M. R. Gibbs, W. G. Stirling, and M. A. Adams, Europhys. Lett. **43**, 422 (1998).
[11] J. V. Pearce, R. T. Azuah, B. Fåk, A. R. Sakhel, H. R. Glyde, and W. G. Stirling, J. Phys.: Condens. Matter **13**, 4421 (2001).
[12] R. P. Feynman and M. Cohen, Phys. Rev. **102**, 1189 (1956).
[13] J. Ruvalds and A. Zawadowski, Phys. Rev. Lett. **25**, 333 (1970).
[14] A. Zawadowski, J. Solana, and J. Ruvalds, Phys. Rev. A **5**, 399 (1972).
[15] H. W. Jackson, Phys. Rev. A **8**, 1529 (1973).
[16] K. Bedell, D. Pines, and A. Zawadowski, Phys. Rev. B **29**, 102 (1984).
[17] H. Glyde, in *Condensed Matter Theories*, edited by L. Blum and F. B. Malik (Plenum, New York, 1993), Vol. 8, p. 159.
[18] K. J. Juge and A. Griffin, J. Low Temp. Phys. **97**, 105 (1994).
[19] F. Pistolesi, Phys. Rev. Lett. **81**, 397 (1998).
[20] J. Szwabinski and M. Weyrauch, Phys. Rev. B **64**, 184512 (2001).
[21] E. Krotscheck, J. Low Temp. Phys. **113**, 509 (1998).
[22] H. R. Glyde, *Excitations in Liquid and Solid Helium* (Oxford University Press, New York, 1994).
[23] H. R. Glyde, Phys. Rev. B **45**, 7321 (1992).
[24] A. Griffin, *Excitations in a Bose-Condensed Liquid* (Cambridge University Press, New York, 1993).
[25] H. R. Glyde, Phys. Rev. Lett. **75**, 4238 (1995).
[26] P. A. Whitlock and R. M. Panoff, Can. J. Phys. **65**, 1409 (1987).
[27] E. H. Graf, V. J. Minkiewicz, H. Bjerrum-Møller, and L. Passell, Phys. Rev. A **10**, 1748 (1974).
[28] N. N. Bogoliubov, J. Phys. (USSR) **9**, 23 (1947).
[29] N. M. Hugenholtz and D. Pines, Phys. Rev. **116**, 489 (1959).
[30] G. D. Mahan, *Many Particle Physics* (Plenum, New York, 1981).
[31] A. A. Abrikosov, L. P. Gorkov, and I. Ye. Dzyaloshinskii, *Methods of Quantum Field Theory in Statistical Physics* (Prentice–Hall, Englewood Cliffs, NJ, 1963).